Earth History and Biodiversity 6 (2025) 100035

Contents lists available at ScienceDirect

Earth History and Biodiversity

journal homepage: www.sciencedirect.com/journal/earth-history-and-biodiversity/

Plants as a proxy for monsoon reconstruction – a case study from the Eocene of East Asia

Olesia V. Bondarenko

Federal Scientific Center of the East Asia Terrestrial Biodiversity, Far Eastern Branch, Russian Academy of Sciences, Prospect Stoletiya 159, Vladivostok 690022, Russia

ARTICLE INFO

Keywords:
Patterns
Gradients
Trends
Seasonality
Monsoon
Atmospheric circulation

ABSTRACT

Eocene precipitation patterns of eastern Eurasia are studied in focus on potential imprints of monsoonal circulation. Based on the application of the Coexistence Approach (CA) on 239 palaeofloras, three precipitation variables are reconstructed and six derived monsoon indices are tested for the early, middle and late Eocene. Under the Eocene greenhouse and diverging palaeogeography, atmospheric circulation and precipitation patterns fundamentally differed from modern. Our reconstruction reveals mainly zonal patterns and significantly higher-than-present precipitation at high and mid-latitudes, with means being highest in the early Eocene. The monsoon indices calculated from CA data yield ambiguous evidences for monsoon circulation during the Eocene. For East Asia, most data suggest a weak or absent summer monsoon, with the medians of the Eocene index values being at the lower ends or below typical modern values for monsoonal conditions. Moreover, they consistently indicate the absence of a winter monsoon, probably related to a weak or absent Siberian High throughout the Eocene. For sites located on the Indian Plate, the indices considered here yield contradictory results. The monsoon indices have their strengths and flaws and hence complemental application of various different indices is proven useful.

1. Introduction

Fossil plant remains are often used as a proxy for reconstructing climate from the Cretaceous to the Quaternary because they are widespread in palaeontological records and directly related to climate. Asia plays a significant role in shaping the global climate system and exerts a significant influence on major planetary changes in atmospheric circulation. Data for East Asia are the key to analyzing atmospheric and oceanic circulation patterns in the geological past at the continental scale. They are also essential for understanding environmental patterns such as monsoons, atmospheric pressure, the Northern Hemisphere's atmospheric circulation system as a whole, and the impact of these factors on the biosphere. In eastern Eurasia, climate and prevailing precipitation patterns are connected to the history of the East Asian Monsoon System (EAMS), complicated by tectonic movements and a shifting palaeogeography (An et al., 2001).

The Eocene is generally assumed to be characterized by a distinctly warm climate, with global mean temperatures thought to be considerably higher than in any other period of the Cenozoic (Greenwood and Wing, 1995; Zachos et al., 2008; Huber and Caballero, 2011; Westerhold et al., 2020). The climatic conditions of the Eocene have been well described using proxy data from either isotope data from shallow marine to deep sea sediments or continental minerals and floras from both North America and Europe (Greenwood and Wing, 1995; Mosbrugger et al., 2005; Wing et al., 2005; Zachos et al., 2008; Greenwood et al., 2010; Utescher et al., 2011). Little is quantitatively known about the southern part of East Asia, except for a few studies in China (e.g. He and Tao, 1997; Su et al., 2009; Yao et al., 2009; Wang et al., 2010; Quan et al., 2011, 2012a, b) and India (Srivastava et al., 2012; Khan et al., 2014; Licht et al., 2014; Shukla et al., 2014). Even fewer quantitative data are available for the northern (Russian Far East – RFE) and continental (Siberia and Kazakhstan) parts. Since quantitative palaeoclimate estimates are essential for understanding these deep time climate conditions, the paucity of studies from East Asia clearly hinders our ability to understand and model the Eocene climate in a global context (Shellito and Sloan, 2006; Huber and Goldner, 2012). Meanwhile, the Eocene was a highly active period in Asian tectonics, with events such as the India-Eurasian collision and associated uplift of the Tibetan Plateau (Tapponnier et al., 2001; Dupont-Nivet et al., 2008; Wang et al., 2008, 2014; Molnar et al., 2010), and the westward retreat of the Paratethys Sea from the Tarim Basin (Bosboom et al., 2011, 2014a, 2014b; Sun et al., 2016). These events would have increased the land-sea thermal

E-mail address: laricioxylon@gmail.com.

https://doi.org/10.1016/j.hisbio.2025.100035
Received 31 August 2025; Received in revised form 24 October 2025; Accepted 12 November 2025
Available online 14 November 2025

contrast and could have initiated the Asian monsoon. Therefore, the Eocene may have been a critical time interval for the onset of EAMS, but it was only recently that geological records and numerical simulations have suggested that the Asian monsoon may have existed during the Eocene (Quan et al., 2012a, 2014; Huber and Goldner, 2012; Wang et al., 2013; Licht et al., 2014; Meng et al., 2018). Evidence from aeolian sediments, lithological and palaeobotanical records reveal that a climate transformation from a dominantly planetary to a monsoon dominated circulation pattern occurred roughly in the time-span from the late Oligocene to early Miocene (Liu et al., 1998; Guo et al., 2002, 2008; Sun and Wang, 2005). Jacques et al. (2013) looked at how monsoon indices behave at the global scale using modern climate data and a geographical information system, and proposed a method to describe palaeomonsoons. The emergence and evolution of EAMS is a topic that has attracted considerable research effort, but limitations of proxy data, coupled with the diversity of definitions and indices characterizing monsoon phenomena, have generated much debate. Recently, based on 110 floras, detailed precipitation gradients and patterns were reconstructed (Bondarenko and Utescher, 2024) along the Pacific coast of Eurasia in space and time to trace climate seasonality for the early and late Paleocene, and early Eocene. According to Bondarenko and Utescher (2024), the early Paleogene records could not be interpreted in terms of a monsoonal type of climate. So, despite the long research history, the question of the emergence of EAMS still remains controversial and debatable. Moreover, there is no Eocene-scale precipitation reconstructions of Asia as a palaeocontinent. These regional data will provide extensive material for understanding the evolution of Earth's climates in the geological past and for developing a general theory of planetary climate as a basis for predicting its changes in the near and distant future.

So far there is considerable confusion in the scientific literature about what constitutes a monsoon. The monsoon is a complex climatic phenomenon, so complex that there is still debate about the causes and mechanisms that lead to what we see in monsoonal regions today (for more details cf. An et al. 2015 and discussions therein). Technically, monsoons are nothing more than a seasonal change in wind direction (Ramage, 1971), associated with marked seasonal variations in precipitation. Sometimes the strength and direction of palaeowinds can be reconstructed, but this is generally impossible to determine from palaeobotanical data. For this reason, palaeoclimate reconstructions are mainly based on the ratio of rainy and dry season precipitation, as well as various indices based on the data available from plant proxies.

The present-day EAMS impacting eastern Asia comprise the East Asian Monsoon (EAM) and the South Asian Monsoon (SAM). The monsoons have clear differences (Molnar et al., 2010). The SAM is characterized by dry winters and wet summers, with temperatures being highest in May to early June, before the onset of the rainy season (Molnar et al., 2010). The EAM is characterized by cold and dry conditions in the cold season evolving under the influence of the Siberian High and affecting large parts of eastern Asia, and a warm and wet season setting on in late spring to early summer when a low-pressure cell forms over Siberia allowing the advection of moist air from the south (Molnar et al., 2010). At present, both systems affect different parts of Asia. The SAM mainly influences northern India and the northeastern Indian Ocean, while the EAM is mainly confined to China, the Korean Peninsula, and southern Japan (Molnar et al., 2010). EAM and SAM are also driven by specific orographic factors that cause specific precipitation patterns, not entirely understood so far. Moreover, the monsoonal character of the EAM has been questioned (for more details Spicer et al. 2016 and Farnsworth et al. 2019 and discussions therein).

Thus, this study addresses the lack of consistent plant-based Eocene-scale precipitation reconstructions. Using Eocene-scale data for Asia as a palaeocontinent, we test several monsoon indices available from palaeobotanical data to trace their changes in space and time, and find spatial anomalies. A comprehensive analysis of several monsoon indices and their anomalies is attempted here to answer the following key question: Did a monsoon-type system exist in the Eocene of East Asia? Our study area includes the eastern part of Eurasia and the Indian subcontinent, ranging from high to lower latitudes (~76–19° N) along the western coast of the Pacific Ocean and deeper into the continent (~57–169° E). For the first time, an extensive regional palaeobotanical record is applied to clarify and discuss the formation/presence of monsoonal patterns at the continental and whole Eocene scales. We compiled 156 published palaeobotanical sites from Western and Eastern Siberia, the RFE, Korea, Kazakhstan, China, India, and Japan. Based on a total of 239 reasonably well-dated micro- and macrofloras, coherent precipitation data sets are presented for three stratigraphic levels, namely for the early, middle and late Eocene, covering the precipitation evolution over a time span of ca. 22 myr. All the precipitation data are reconstructed using a single approach (the Coexistence Approach – CA) applicable on every organ type in the fossil palaeobotanical records.

2. Study area

The palaeobotanical records studied herein originate from 156 localities (Fig. 1, Appendix 1). The Paleogene deposits of China, including the Eocene ones, are widely distributed and generally represent terrestrial facies conditions. The plant-bearing strata of eastern China are mainly of fluvial to lacustrine origin, while in the central and western China, Eocene deposits may contain red-beds and evaporites. The majority of these strata, however, lacks detailed geochronological investigations (Li, 1984). As a result, the ages of many of these floras were initially assigned only to a wide stratigraphical range, such as to an epoch or system level, based on floristic assemblages. This apparently reduces the resolution of palaeoclimatic results, or even casts doubt on their validity in palaeoclimatic modeling (Quan et al., 2012a). Fortunately, recent interdisciplinary studies significantly improved the age constraints in many localities (e.g., Huang et al., 1998; Wang et al., 1999; Miao et al., 2008; Shi et al., 2008; Pei et al., 2009). This provides opportunities to reconstruct palaeoclimates in a better resolution at the stage level (Quan et al., 2012a).

The Paleogene deposits of Russian Far East (RFE) and Eastern Siberia are also widely distributed, and are dominated by non-marine facies. The strata of south RFE comprise volcanic and sedimentary deposits, unconformably overlying Mesozoic basement. The sedimentary facies include fine- to coarse-grained continental clastics and intercalated lignites excavated in several active opencast mines. The sedimentary successions in the individual basins are characterized by numerous unconformities related to regional tectonics and phases of rifting and subsidence (Pavlyutkin and Petrenko, 2010). The Eocene deposits of Eastern Siberia and Northeast Russia are exposed in isolated Cenozoic coastal basins, superimposed on folded basement of the Siberian Platform of differing ages. These include tectonic structures adjacent to the Pacific Ocean (Murukta, Kharaulakh), depressions located in the lower reaches of the Lena River (Sogo, Kengdei, and Kunga Basins), sections of the Tastakh Lake area in the Yana–Indigirka interfluve, sections of Ugol'naya Bay, Rarytkin Ridge, and Anadyr River Basin (northern Koryakiya), and coastal sections of northwestern and central Kamchatka.

To the west, our study area includes the marginal part of the West Siberian Plain, adjacent to the eastern slope of the Ural Mountains in the Tobol and Ob′ river basins. During the Late Cretaceous and Paleogene, this territory formed a single structure with the Turgai Trough located to the south – a strait connecting the epicontinental seas of the Palearctic with the Para-Tethys (Vasilieva and Levina, 2007). Paleogene deposits in this region have wide distribution, and overlap the Paleozoic folded basement, reaching a thickness of 400 m. The rocks are characterized mainly by a terrigenous-siliceous type of sedimentation (Amon, 2001, 2018), therefore calcareous microfossils (foraminifera, nannoplankton) are rare, and the leading role in regional biostratigraphy belongs to dinoflagellate cysts. Paleogene deposits in this area are developed everywhere and are represented by both marine and continental facies. At the same time, marine deposits are the most widespread and fill the

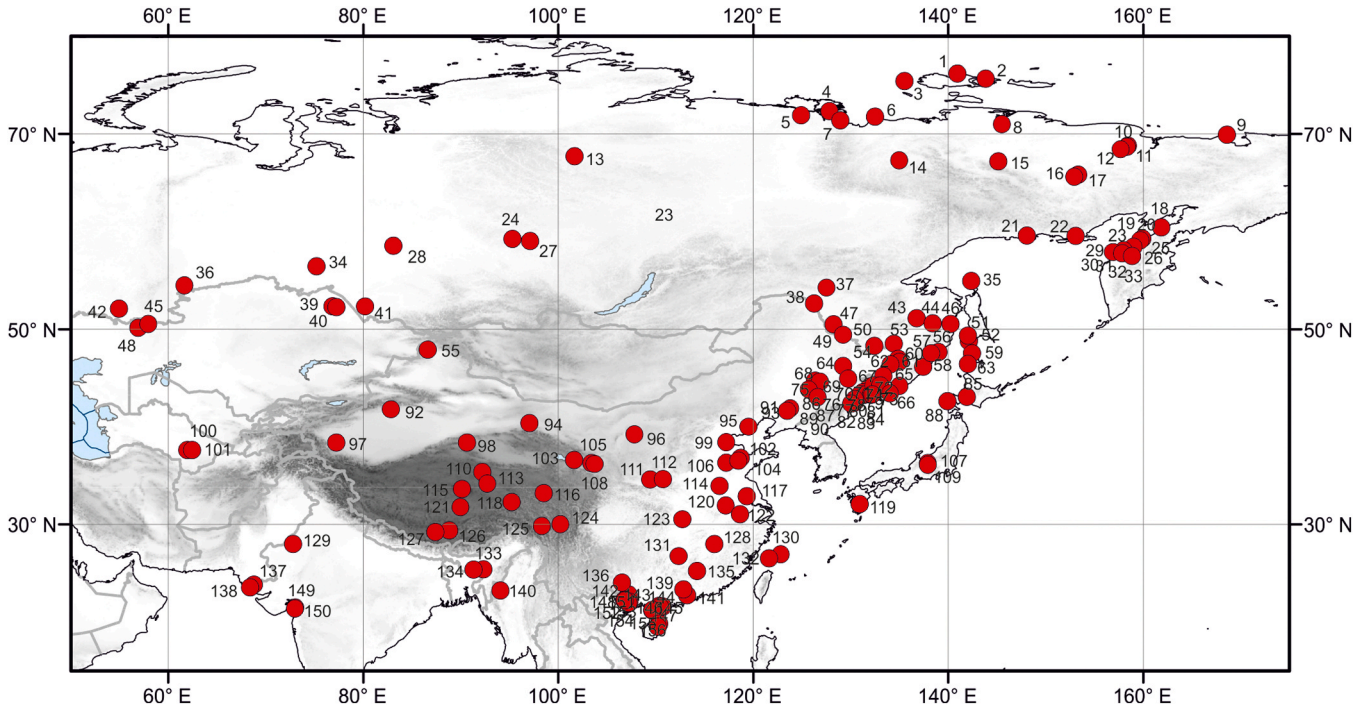

Fig. 1. Map showing the locations of the Eocene floras studied. The localities are listed in Appendix 1.

main part of the Paleogene section, while continental strata occur at the very top of the Paleogene sequence.

The regional stratigraphic correlation chart for single basins (Appendix 1) is adapted from Quan et al. (2012a) for China, Kezina (2005) and Pavlyutkin and Petrenko (2010) for the continental part of the south RFE, Gladenkov et al. (2002) for Sakhalin Island, Gladenkov et al. (2005) for the Kamchatka Peninsula, and Grinenko et al. (1997) for the continental part of the north RFE and Siberia. Age control of the selected Eocene fossil floras of eastern Eurasia is based on a variety of stratigraphic data obtained from radiometric, geochemical and palaeomagnetic dating, well log correlations, and regional sequence-stratigraphical concepts, considering the position of volcanogenic units and main phases of peat forming, vertebrate and invertebrate fauna, mammals, reptiles, mollusks, gastropods, ostracods, foraminifera, calcareous nannofossils, charophytes, and regional and inter-regional pollen zonation (Appendix 1). The stratigraphic schemes of the Russian Far East and Siberia have been tied to the International Stratigraphic Chart (Grinenko et al., 1997; Gladenkov et al., 2002, 2005; Kezina, 2005; Pavlyutkin and Petrenko, 2010; Cohen et al., 2020) and allows for dating the flora-bearing horizons at the stage level. For some of the floras, stratigraphic ages are better constrained (cf. Appendix 1). All in all, ca. 95 % of the floras can be assigned at stage-level, while ca. 5 % have epoch-level assignment.

3. Material and method

3.1. The floral record

The palaeobotanical record is diverse and has been subject to extensive taxonomic studies (cf. Appendix 1 for references). All palaeofloras considered here were carefully re-evaluated regarding the validity of taxonomic identifications and Nearest Living Relatives (NLRs) of the fossil taxa. We analyse a total of 239 floras including 174 palynofloras (PF), 64 leaf floras (LF) and one carpoflora (CF) with respect to palaeoclimate considering three time slices, namely the early, middle, and late Eocene. The floras cover a total time-span of ca. 22 myr, ranging from Ypresian (55.8 Ma) to Priabonian (33.9 Ma).

The assignment of the palaeofloras to the three time slices considered here is done on the basis of stratigraphic information available in literature and compiled in Appendix 1 and 2. In many cases, flora-bearing horizons originate from longer successions that are tied to regional stratigraphy and cover the entire Eocene – 14 sites (e.g., Alchan, Bikin, Fushun, Lanzhou, etc.) thus facilitating a consistent sample selection. 29 floristic levels contain both micro- and macrofloras. The single floras are listed in Appendix 1, together with information on basin provenience, type of flora, stratigraphic age, method of dating, and references. The complete floral lists, assigned NLRs and their climatic requirements are given in Appendix 2. For the early Eocene, a total of 83 floras (67 PF and 16 LF) is at disposal, all within the range from 21.25 to 76.06° N and from 61.71 to 145.60° E. For the middle Eocene, the compilation comprises 83 floras (57 PF, 25 LF and 1 CF) within the range from 19.38 to 75.53° N and from 58.00 to 168.66° E. The late Eocene record includes 73 floras (50 PF and 23 LF) covering the range from 20.60 to 71.70° N and from 57.00 to 161.96° E.

3.2. Application of the Coexistence Approach (CA)

To reconstruct quantitative precipitation data from the plant fossil record the Coexistence Approach – CA (Mosbrugger and Utescher, 1997; Utescher et al., 2014) was applied. This approach is organ-independent, so that both macro- and microfossil floras are eligible as long as their modern botanical affinities are determinable (Mosbrugger and Utescher, 1997; Utescher et al., 2007; Bruch et al., 2011). For a detailed description of the method the reader is referred to the original papers describing the procedure (Mosbrugger and Utescher, 1997; Utescher et al., 2014). As source for climatic requirements of extant plant taxa, data sets from the Palaeoflora Database (Utescher et al., 2024) were used. Floral lists with corresponding NLRs employed in this study and their climatic requirements are made available in Appendix 2. For the application of the CA, the published flora lists and NLR interpretations of the fossil record were revisited, updated and homogenized.

In this study, four precipitation variables are reconstructed, namely mean annual precipitation (MAP), mean precipitation of driest, wettest and warmest months (MPDRY, MPWET and MPWARM). In the CA, at

least 10 NLR taxa contributing with climate data are required to obtain reliable results (Mosbrugger and Utescher, 1997). Here, 5–127 (mean 33.9) taxa contribute to determining the coexistence intervals – CIs (Appendix 3). In total, 395 taxa of NLRs with their climatic requirements were used (Appendix 4).

The climatic resolution of the CA results also depends on the taxonomical level of the NLR assignment (Mosbrugger and Utescher, 1997). For the Eocene floras, genera or family levels for NLRs were used (Appendix 2). Cosmopolitan and subcosmopolitan taxa were not considered in CA analysis. Monotypic taxa (*Eucommia ulmoides* Oliv., *Ginkgo biloba* L. and *Sciadopitys verticillata* (Thunb.) Siebold et Zucc.) were also excluded from the analysis. For the monotypic genera (but not monotypic families) we use climate data for (sub)families (cf. Bondarenko and Utescher, 2022, 2024).

To illustrate precipitation patterns and gradients, the floras are allocated to three time intervals: early, middle, and late Eocene. These time intervals are defined according to the international standard. To visualize the results, a series of maps is provided and discussed below. The maps, allowing to trace the evolution of the three precipitation variables (MAP, MPDRY and MPWET) throughout the Eocene, are based on means of CIs for each palaeoflora and averaged for the time intervals regarded, and to compare them with the present-day (Figs. 2–4). The complete set of CIs for all floras and precipitation variables is provided in Appendix 3. To show the Eocene data in the context of modern climate space, a Principal Component Analysis (PCA) was performed using three temperature (mean annual temperature – MAT, cold and warm month mean temperature – CMMT and WMMT) and three precipitation variables (MAP, MPWET and MPDRY) (proxy and station data). The plots are shown for the three most important components, explaining ca. 95 % of the variability in the data (Fig. 5). Complete data sets for the PCA are given in Appendix 5. For the technical preparation of the maps, ArcMAP 10.4 was used.

3.3. Seasonality and monsoon indices

In order to measure monsoon intensity, various indices theoretically can be calculated. Following Jacques et al. (2013), monsoon indices were selected based only on precipitation and temperature parameters which are available in palaeoclimatic reconstructions using CA. Since many variables are not at disposal in the CA, the indices were calculated to estimate monsoon intensity using mean monthly precipitation (Table 1, Figs. 6–10).

In order to determine precipitation seasonality, the mean annual range of precipitation (MARP) was calculated as the difference of MPWET and MPDRY for the time intervals studied. The van Dam index (MPWET – MPDRY) was defined to reconstruct monsoon strength based on palaeoprecipitation results derived from small mammal proxies (van Dam, 2006), however, indeed it repeats the MARP index. The MPWET/MPDRY ratio is also used to estimate precipitation seasonality (Lau and Yang, 1997; Zhang and Wang, 2008). According to Jacques et al. (2011a,b), the ratios of MPWET and MPDRY on MAP are good indicators of the strength of the East Asian Summer Monsoon and the Winter Monsoon, respectively. In order to measure monsoon intensity during the Eocene we used the ratios of MPWET and MPDRY on MAP (RMPWET and RMPDRY). A monsoon sensitivity index (MSI), according to Liu and Yin (2002), based on seasonal temperature and precipitation differences, namely $MSI = (T_S - T_W) \times (R_S - R_W)$, where Ts and Tw are summer and winter mean temperature at the surface, and Rs and Rw are summer and winter mean precipitation, respectively. A monsoon index, roughly comparable to the MSI, monsoon sensitivity high (MSH) was calculated using monthly values in following the assumptions by Liu et al. (2011) as MSH = (WMMT – CMMT) × (MPWARM – MPDRY). Moreover, a new monsoon index is suggested – "EAM proxy" index, which is calculated as sqrt [(MPWET – MPmean) × (MPmean – MPDRY)], where MPmean is mean month precipitation. This index performs well in reflecting modern monsoonal areas in East Asia (Fig. 9). By intersecting WOLDCLIM data (Hijmans et al., 2005) and the polygon bordering the modern region impacted by the EAM (Liu and Shi, 2015), a threshold for monsoonal climate is identified. Using 95 %iles of the data extracted from the intersection, this threshold should exceed 47 to be indicative for monsoonal climate (Fig. 9).

In order to further comparison, the obtained index values against the present-day measured climatic data, the data from 224 meteo stations located within the study area were used (Appendix 6). To visualize the results, a series of maps is provided and discussed below. The maps, allowing to trace the spatio-temporal patterns of the monsoon indices listed above throughout the Eocene, and to compare them with the present-day (Figs. 6–10). The complete set of calculated ratios and indices studied for all floras is provided in Appendix 3. To better reflect the underlying statistics, boxplots are shown for individual variables considering modern non-monsoon and monsoon stations (Müller and Hennings, 2000) and, data obtained for early, middle, and late Eocene sites located in the realm of the extant EAM and those on the Indian Plate (Fig. 11). For the technical preparation of the maps, ArcMAP 10.4 was used.

4. Results

A complete list of taxa for each of the localities, including their NLRs with precipitation requirements, is provided in Appendix 2. Precipitation data calculated for the 239 floras are given in Appendix 3. CA-based precipitation data are obtained from a total of 174 microfloras (mean diversity of taxa contributing with climate data: 36.5, std. 14.2) and 65 macrofloras (mean diversity of taxa contributing with climate data: 26.5, std. 12.3). In the early Eocene, proportions of coexisting NLR taxa vary from 95.1 % (PF Fadeevsky) to 100 % (61 floras); mean value is 99.7 %. In the middle Eocene, proportions of coexisting NLR taxa vary from 94.3 % (PF Litang) to 100 % (51 floras); mean value is 99.6 %. In the late Eocene, proportions of coexisting NLR taxa vary from 92.7 % (PF Kalewa) to 100 % (48 floras); mean value is 99.6 %. Totally, in 160 out of 239 cases, the calculations of all considered variables the proportion of coexisting NLR taxa are 100 %, in 79 cases – from 92.7 % to 99.7 %.

Regarding MAP (Fig. 2, Table 2), in the early Eocene, the upper limits for MAP CIs – 399–2211 mm, lower limits – 866–3151 mm, the mean values of MAPmean range from 803 to 2681 mm (mean 1216 mm). In the middle Eocene, the upper limits for MAP CIs – 503–1438 mm, lower limits – 1096–1438 mm, the mean value of MAPmean range from 800 to 1650 mm (mean 1148 mm). In the late Eocene, the upper limits for MAP CIs – 352–2211 mm, lower limits – 1096–3151 mm, the mean value of MAPmean range from 705 to 3141 mm (mean 1205 mm). Based on the MAP means, three zones can be distinguished.

For MPWET (Fig. 3, Table 2), in the early Eocene the means of CIs range from 145 to 359 mm (mean 207 mm). In the middle Eocene, the means of MPWET CIs range from 147 to 320 mm (mean 204 mm). In the late Eocene, the means of MPWET CIs range from 116 to 389 mm (mean 200 mm). Based on the MPWET means, three zones can be distinguished.

For MPDRY (Fig. 4, Table 2), in the early Eocene the means of CIs range from 16 to 101 mm (mean 44 mm). In the middle Eocene, the means of MPDRY CIs range from 24 to 61 mm (mean 37 mm). In the late Eocene, the means of MPDRY CIs range from 10 to 101 mm (mean 39 mm). Based on the MPDRY means, three zones can be distinguished.

The MARP (Fig. 6, Table 2) in the early Eocene vary in range 112–306 mm (mean 163 mm). In the middle Eocene, the MARP ranges from 86 to 287 mm (mean 167 mm). In the late Eocene, the MARP ranges from 90 to 349 mm (mean 163 mm).

All localities are characterized by a marked difference in the MPWET/MPDRY ratio, which mainly varies from 3:1–8:1, but for some floras even from 10:1–16:1 (Table 2, Appendix 3). In the early Eocene, the ratio ranges from 3:1–12:1, the highest values are obtained for Ozero Toni LF (12:1) and Alchan PF (10:1). In the middle Eocene, the ratio

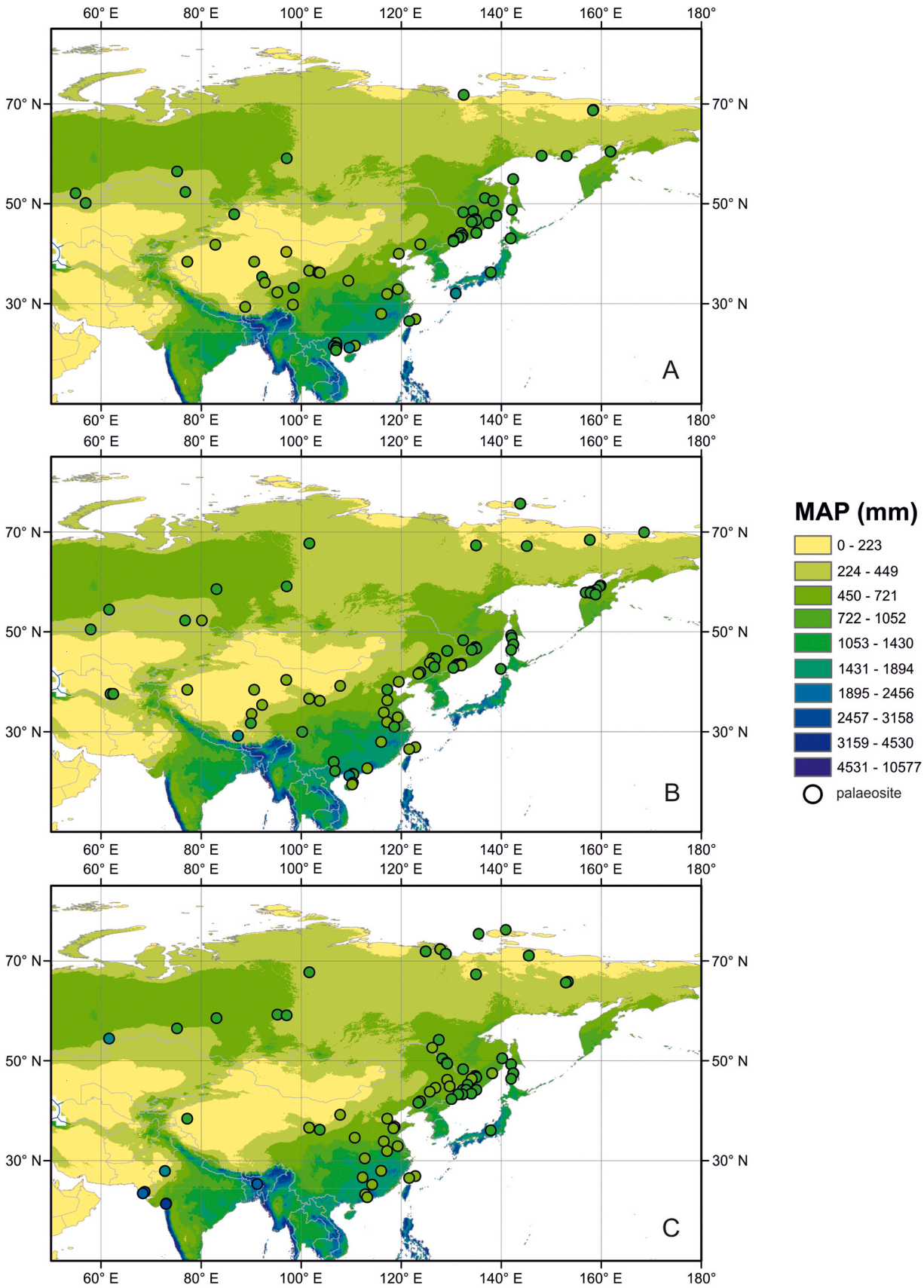

Fig. 2. Eocene mean annual precipitation (MAP) patterns based on means of coexistence intervals obtained for each palaeoflora, plotted on present-day MAP calculated using WORLDCLIM (Hijmans et al., 2005). A: early Eocene; B: middle Eocene; C: late Eocene.

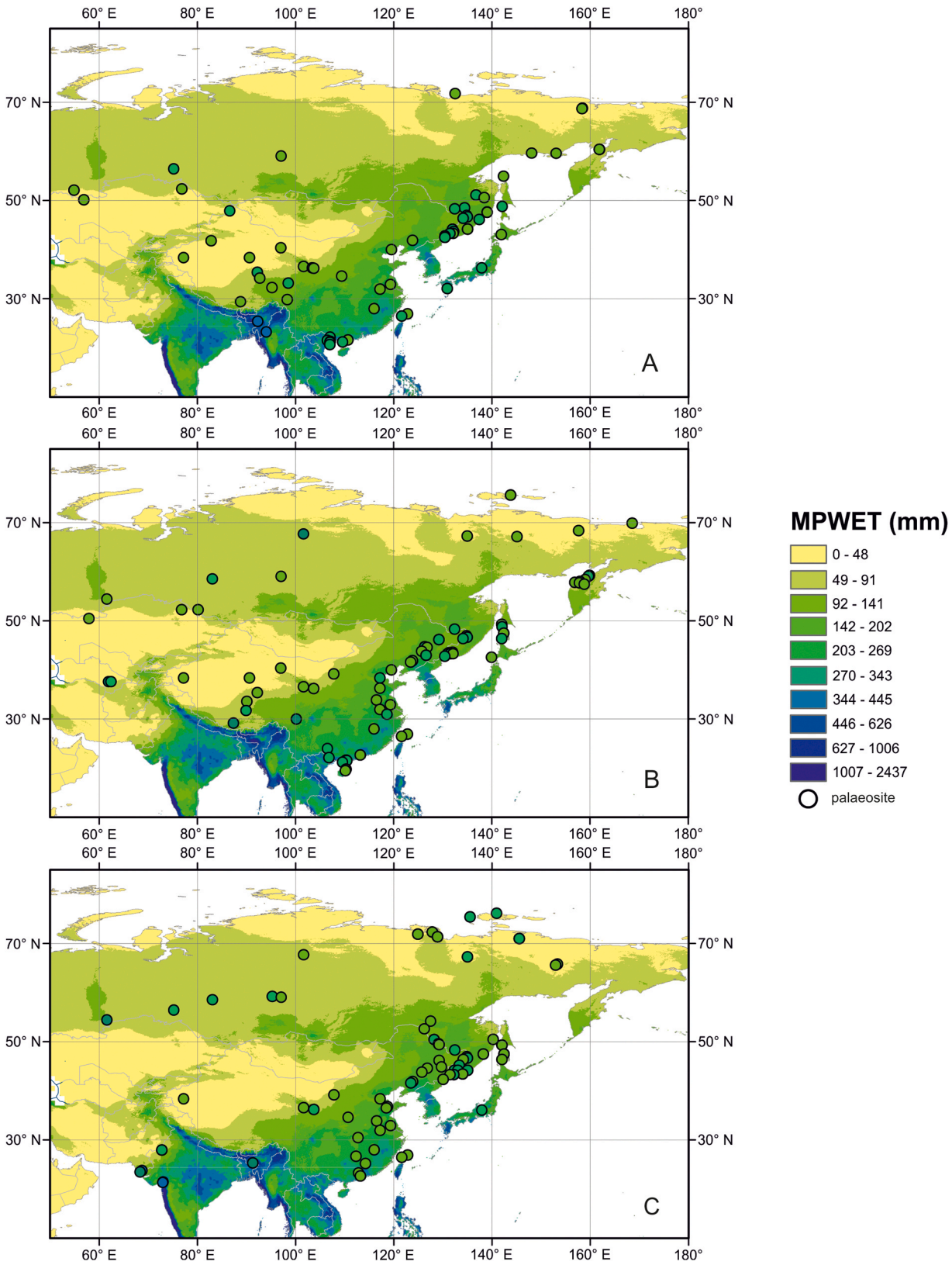

Fig. 3. Eocene mean precipitation of wettest month (MPWET) patterns based on means of coexistence intervals obtained for each palaeoflora, plotted on present-day MPWET calculated using WORLDCLIM (Hijmans et al., 2005). A: early Eocene; B: middle Eocene; C: late Eocene.

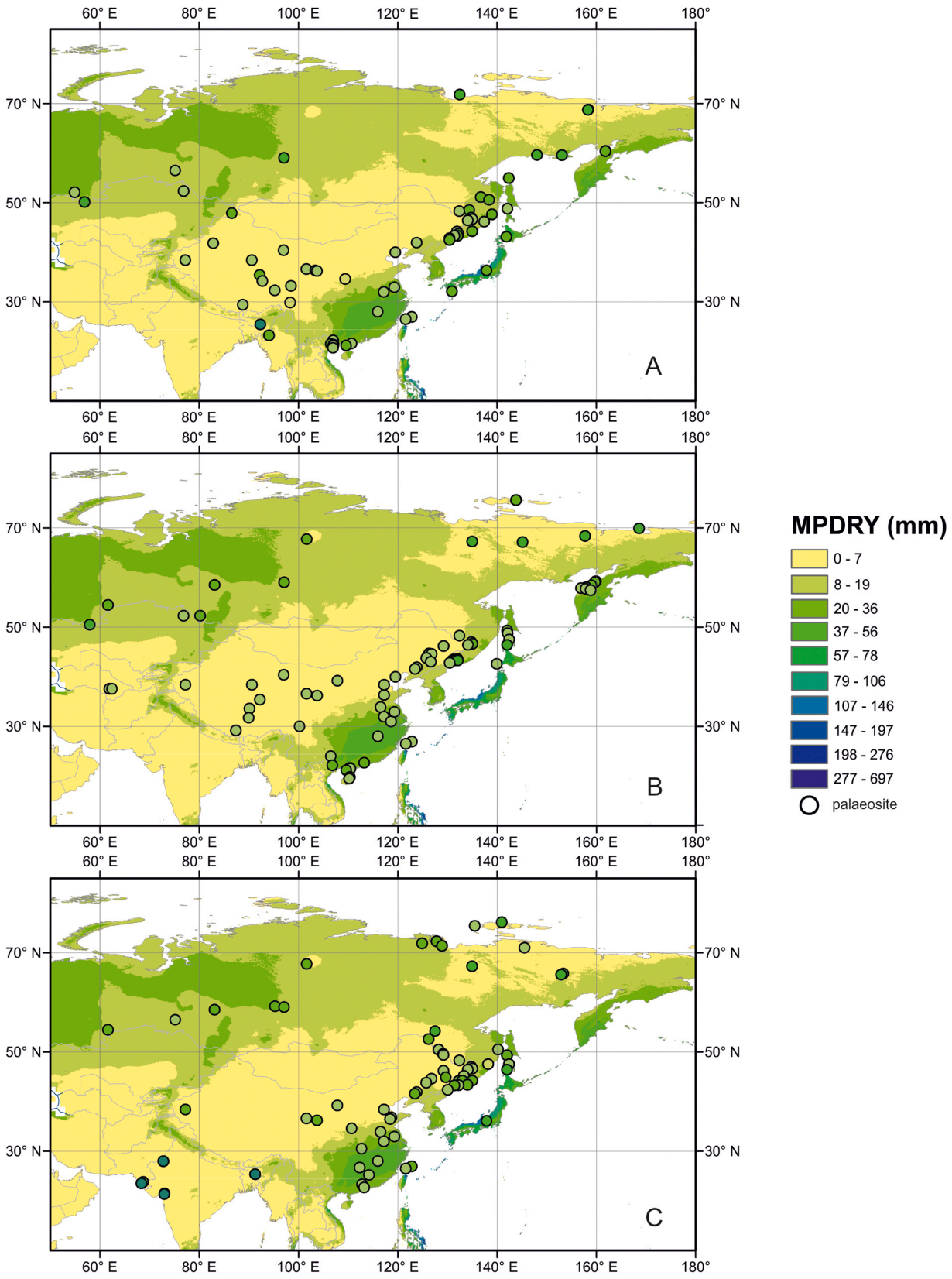

Fig. 4. Eocene mean precipitation of driest month (MPDRY) patterns based on means of coexistence intervals obtained for each palaeoflora, plotted on present-day MPDRY calculated using WORLDCLIM (Hijmans et al., 2005). A: early Eocene; B: middle Eocene; C: late Eocene.

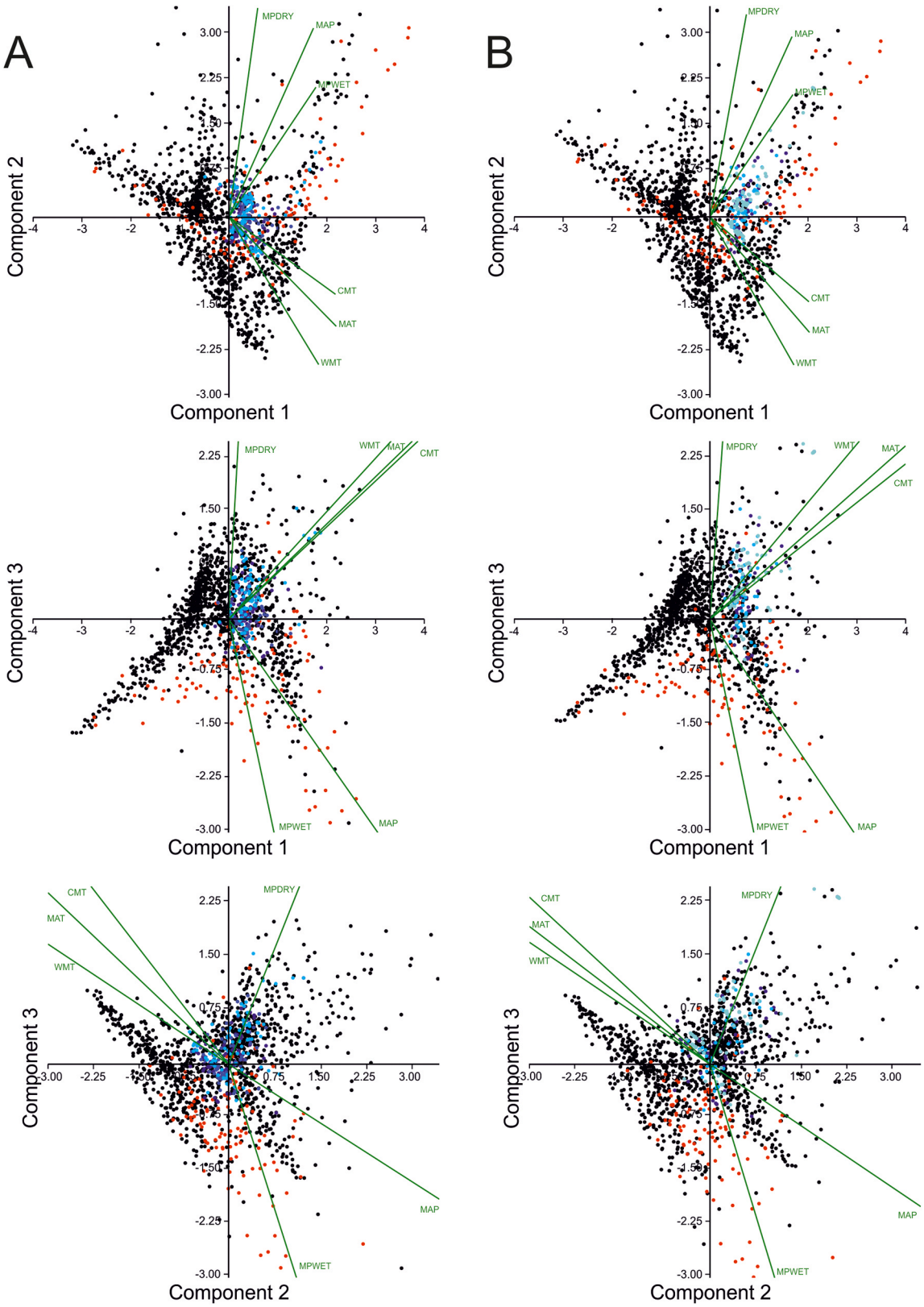

Fig. 5. Principal Component Analysis (PCA) using three temperature (mean annual temperature – MAT, cold and warm month mean temperature – CMMT and WMMT) and three precipitation variables (mean annual precipitation – MAP, mean precipitation of wettest and driest months – MPWET and MPDRY) (proxy and station data) showing the position of Eocene data in the modern climate space (as defined by the station data from Müller and Hennings 2000): non-monsoonal sites – in black dots, monsoonal sites – in red and fossil sites– in blue (scale dark to light = early to late Eocene). A: using minima of coexistence intervals; B: using maxima of coexistence intervals.

Table 1
Monsoon indices are using in this study.

Name definition, literature source	MARP or van Dam index (mm) (van Dam, 2006)	MPWET/MPDRY ratio (Lau and Yang, 1997; Zhang and Wang, 2008)	RMPWET (%) (Jacques et al., 2011a, b)	RMPDRY (%) (Jacques et al., 2011a, b)	MSH (Liu et al., 2011)	"EAMS proxy" index (this study)
Formula for calculation	MPWET – MPDRY	MPWET/MPDRY	MPWET/MAP × 100	MPDRY/MAP × 100	(WMMT – CMMT) × (MPWARM – MPDRY)	sqrt [(MPWET – MPmean) × (MPmean – MPDRY)]
modern non-monsoon						
min	0	1	0	0	0	0
max	952	466	64.7	7.6	7770	461
mean	11	18	17.0	3.2	1213	52
modern monsoon						
min	29	2	10.1	0	65	13
max	2682	1321	39.3	5.8	23870	1262
mean	347	28	21.5	1.0	3071	164
late Eocene						
min	90	3	12.4	1.2	74	45
max	349	16	23.0	5.2	3408	168
mean	163	6	16.9	3.2	1720	78
middle Eocene						
min	86	2	11.8	2.1	553	43
max	287	11	22.5	5.9	3039	136
mean	167	6	17.9	3.2	1811	79
early Eocene						
min	112	3	12.5	1.9	74	51
max	306	12	24.1	5.4	4313	147
mean	163	5	17.3	3.6	1525	77

Note: The monsoon and non-monsoon types of the modern climate are defined based on the Koeppen–Geiger classification.

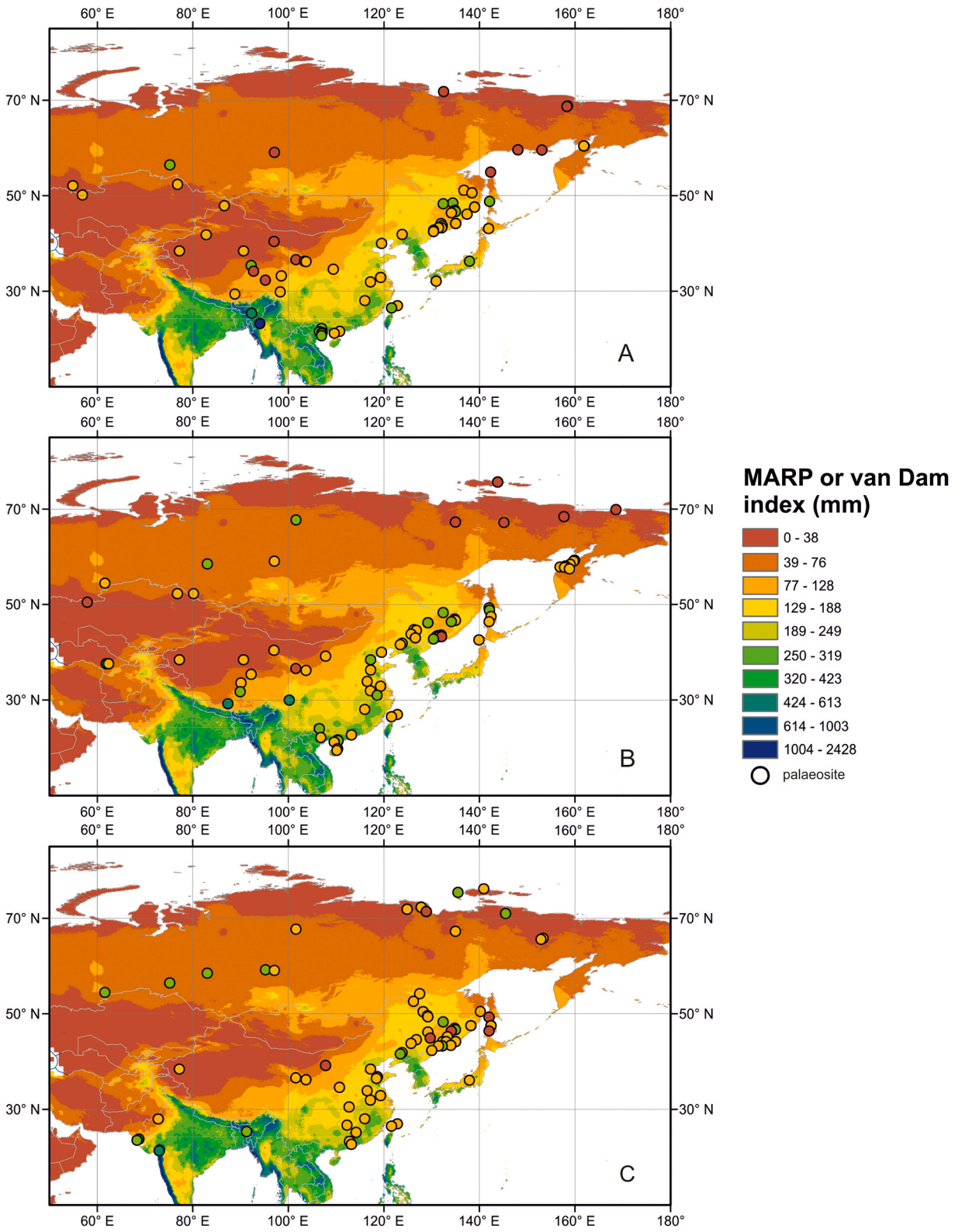

Fig. 6. Eocene mean annual range of precipitation (MARP) patterns obtained for each palaeoflora, plotted on present-day MARP calculated using WORLDCLIM (Hijmans et al., 2005). A: early Eocene; B: middle Eocene; C: late Eocene.

ranges from 2:1–11:1, the highest values are obtained for Litang PF (11:1) and AS_Lazi PF (10:1). In the late Eocene, the ratio ranges from 3:1–16:1, the highest values are obtained for Weinan LF (16:1), Yen My PF, Le Loi PF and Gieng Day PF (13:1), as well Hunchun PF, Markam LF and Kalewa PF (10:1).

The calculated RMPWET values (Fig. 7, Table 2) in the early Eocene vary from 12.5 % (Gurha LF) to 24.1 % (Ozero Toni LF). In the middle Eocene, the values are 11.8 % (AS_Karakol LF) to 22.5 % (Zhenjiang PF and Shigu PF). In the late Eocene, the values are 12.4 % (Kalewa PF) to 23.0 % (Pavlovka9035-D PF).

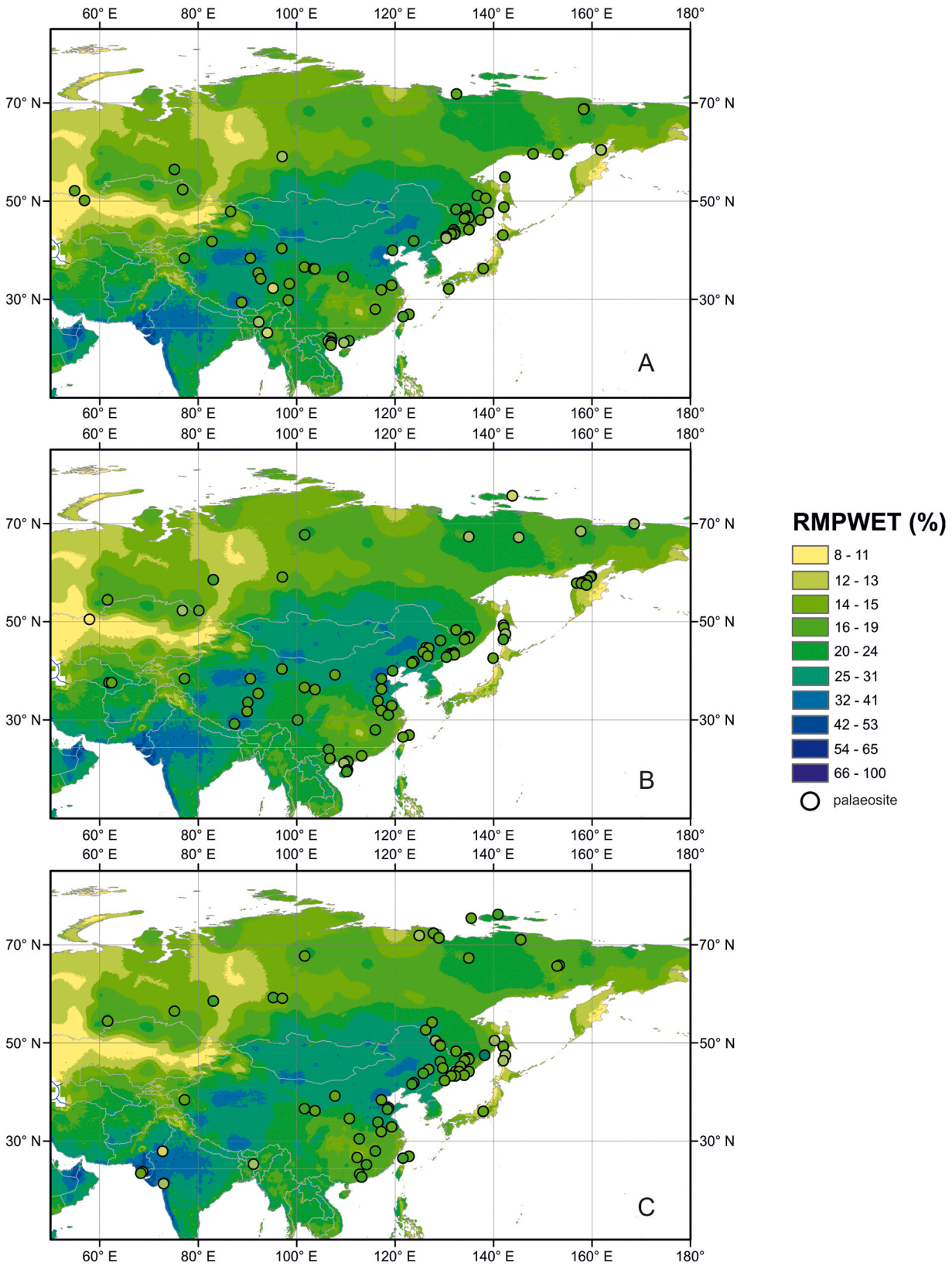

Fig. 7. Eocene patterns of the ratio of mean precipitation of wettest month (RMPWET) obtained for each palaeoflora, plotted on present-day data calculated using WORLDCLIM (Hijmans et al., 2005). A: early Eocene; B: middle Eocene; C: late Eocene.

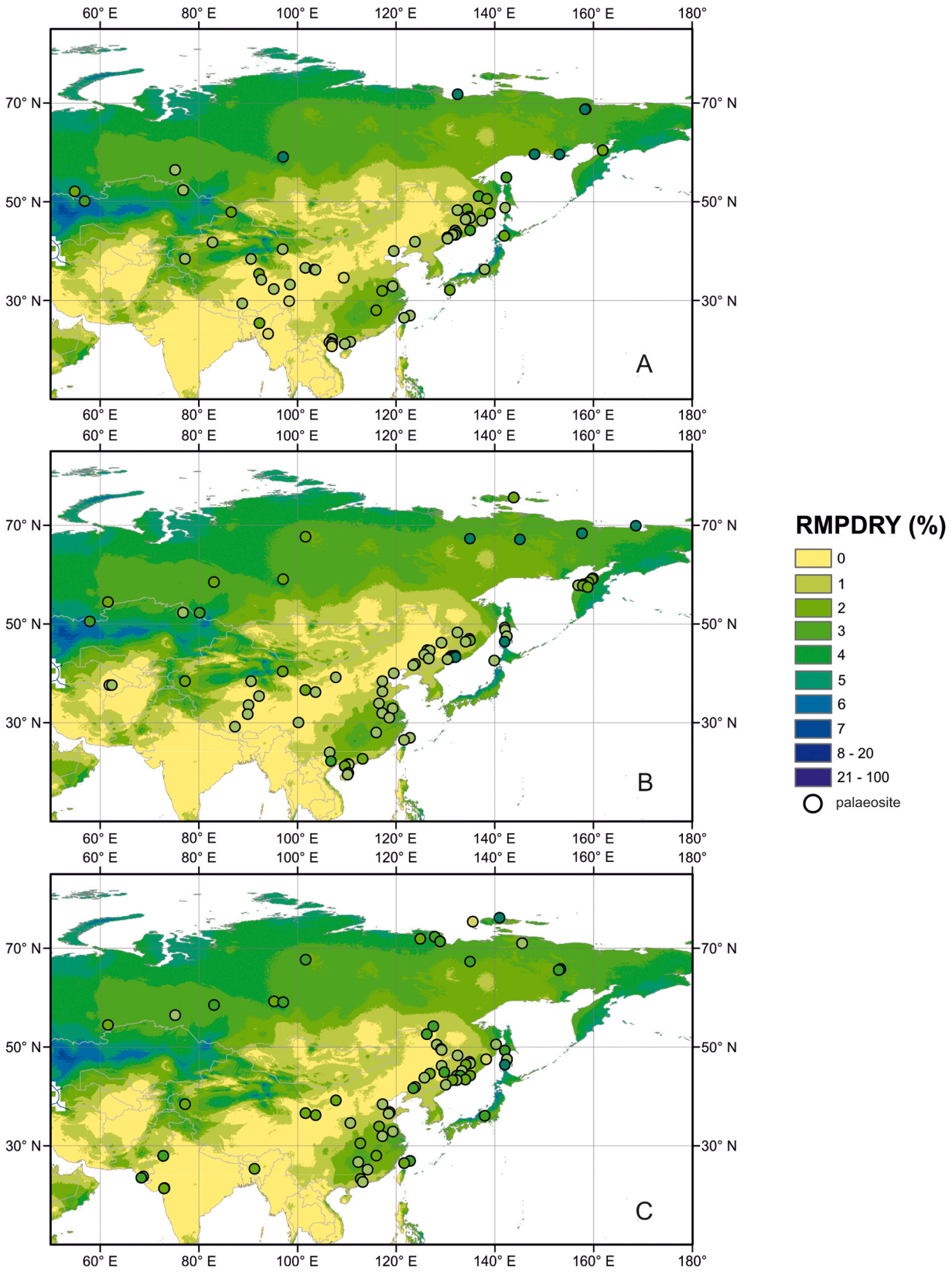

Fig. 8. Eocene patterns of the ratio of mean precipitation of driest month (RMPDRY) obtained for each palaeoflora, plotted on present-day data calculated using WORLDCLIM (Hijmans et al., 2005). A: early Eocene; B: middle Eocene; C: late Eocene.

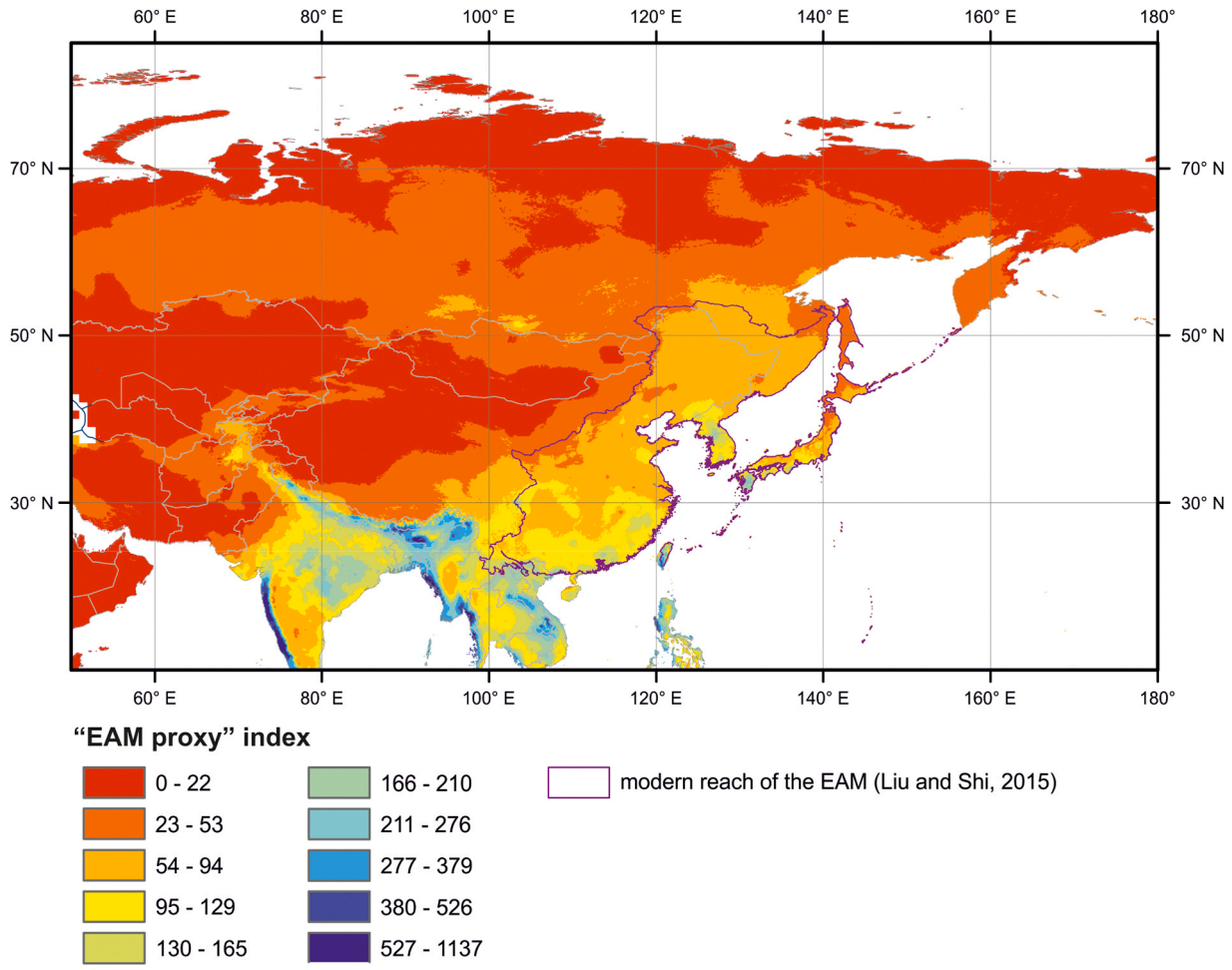

Fig. 9. Modern pattern of the presently proposed monsoon index ("EAM proxy") calculated using WORLDCLIM (Hijmans et al., 2005).

The calculated RMPDRY values (Fig. 8, Table 2) in the early Eocene range from 1.9 % (Ozero Toni LF) to 5.4 % (Ozero Toni PF). In the middle Eocene, the values are 2.1 % (Luchegorsk540/541 PF, Jianglang LF, Litang PF, and AS_Lazi LF) to 5.9 % (Shkotovo PF). In the late Eocene, the values are 1.2 % (Weinan LF) to 5.2 % (Buorkhaya213 PF, Kolyma1 PF, Krestovka107 PF, Kava4 PF, and Lankovaya PF).

The MSH value for the Eocene of East Asia varies from 66.6 (early Eocene Panandhro PF) to 4180.0 (early Eocene Belkovsky PF) (Table 2, Appendix 3).

Our new index (Fig. 10, Table 2) in the early Eocene varies from 51 (Ozero Toni PF) to 148 (Akri PF). In the middle Eocene, the values are 43 (AS_Karakol LF) to 136 (AS_Lazi LF). In the late Eocene, the values are 45 (Nangqian PF) to 168 (Kalewa PF).

5. Discussion

5.1. Eocene precipitation patterns

The first thing that catches the eye when looking at a series of the maps for all precipitation variables (Figs. 2–4) is that the Eocene precipitation patterns of East Asia are fundamentally different from the modern ones. Based on MAP means (Fig. 2), our reconstruction generally reveals that at high and mid-latitudes the Eocene MAP was significantly higher than the present-day values. The highest mean value of all calculated MAP is obtained for the early Eocene.

For the High Arctic, in the early Eocene CI means indicate wet conditions in the order of (1000) 1200–1300 (1500) mm for MAP. The values correspond to CA-based MAP values of East Asia in the early Eocene (1200–1300 mm) reconstructed by Bondarenko and Utescher (2024). These data are also close to CLAMP-based precipitation estimates for early Eocene floras of northern Yakutia and the Far East (MAP ca. 1200 mm, cf. Budantsev, 1999). In the middle Eocene, our reconstruction shows a minor decreasing trend of MAP ranging between (1000) 1100–1200 (1400) mm. According to Akhmetiev (2004), in the middle Eocene, the same climatic zonality that was traced for the Paleocene and early Eocene floras continued to be preserved. He indicated the MAP as 1000–1500 mm. In the late Eocene, our data also indicate very high values of MAP varying from 1100 to 1300 mm. According to Akhmetiev (2004), a minor decline of MAP occurred in the late Eocene – the values vary from 1100 to 1200 mm

As regards the mid-latitudes of East Asia, our reconstruction reveals a lower precipitation level of 800–1100 mm for the sites located between ~100–145° E and ~25–45° N, throughout the whole Eocene. In the western continental part (west of ~100° E), i.e. near the coast of Tethys, more humid conditions are reconstructed with MAP at 1100–1500 mm. The CA-based MAP values reconstructed by Bondarenko and Utescher (2024) for East Asia in the early Eocene south of 45° N are also not exceeding ca. 1100 mm. For the early Eocene of the northeastern China, Quan et al. (2012b) reconstructed MAP ranges from 373 to 1577 mm, with more specific ranges of 1000–1100 mm. For the early Eocene of China, Quan et al. (2012a) gave MAP values ranging from 735 to 1632 mm, with more specific ranges of 1100–1200 mm. According to Quan et al. (2012a), the climates apparently did not considerably change in the middle Eocene, compared to the early Eocene, with persistently equable warm temperatures and relatively high precipitations. The precipitations significantly changed in the late Eocene,

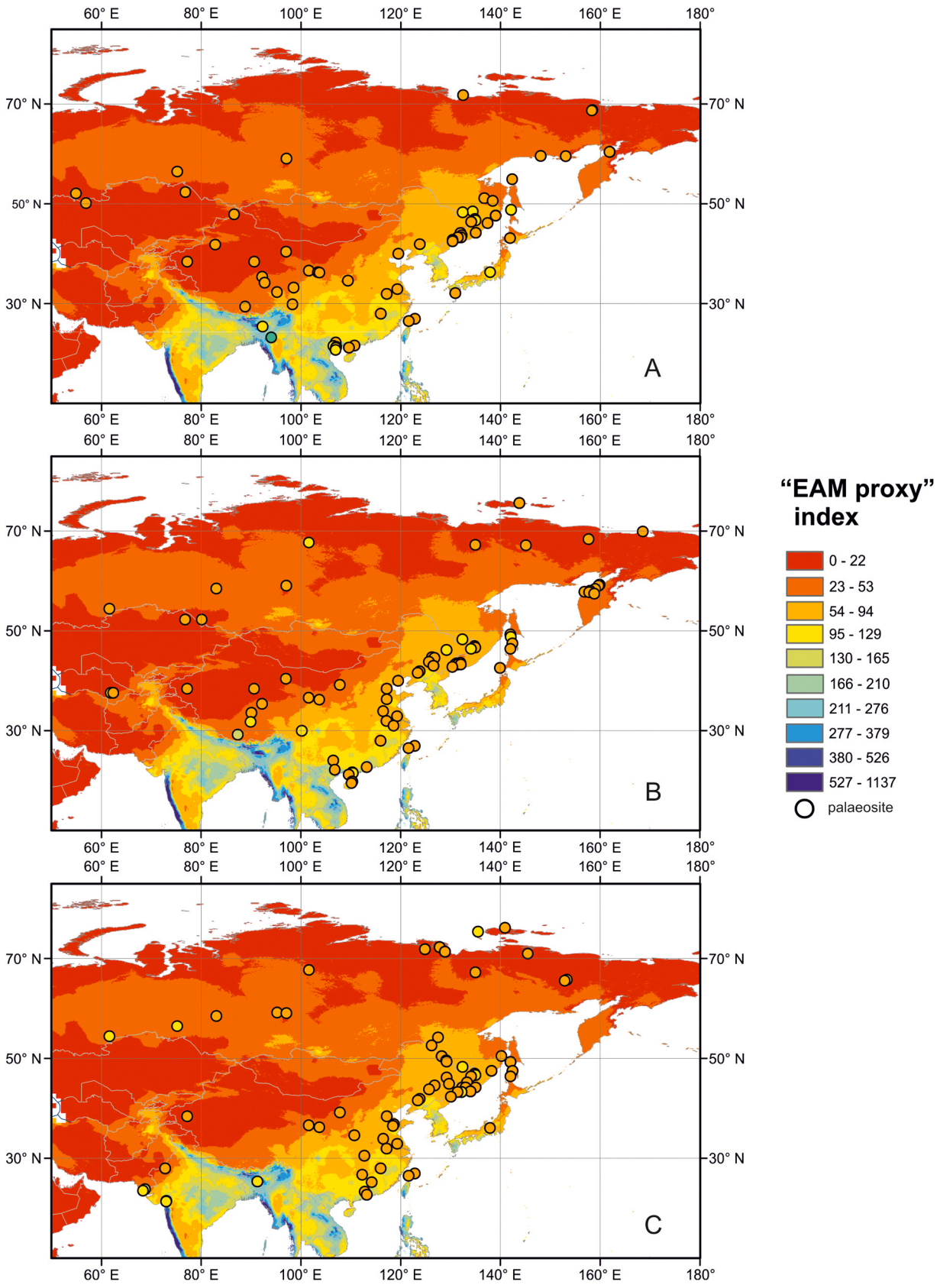

Fig. 10. Eocene patterns of the "EAM proxy" index obtained for each palaeoflora, plotted on present-day data as shown in Fig. 9. A: early Eocene; B: middle Eocene; C: late Eocene.

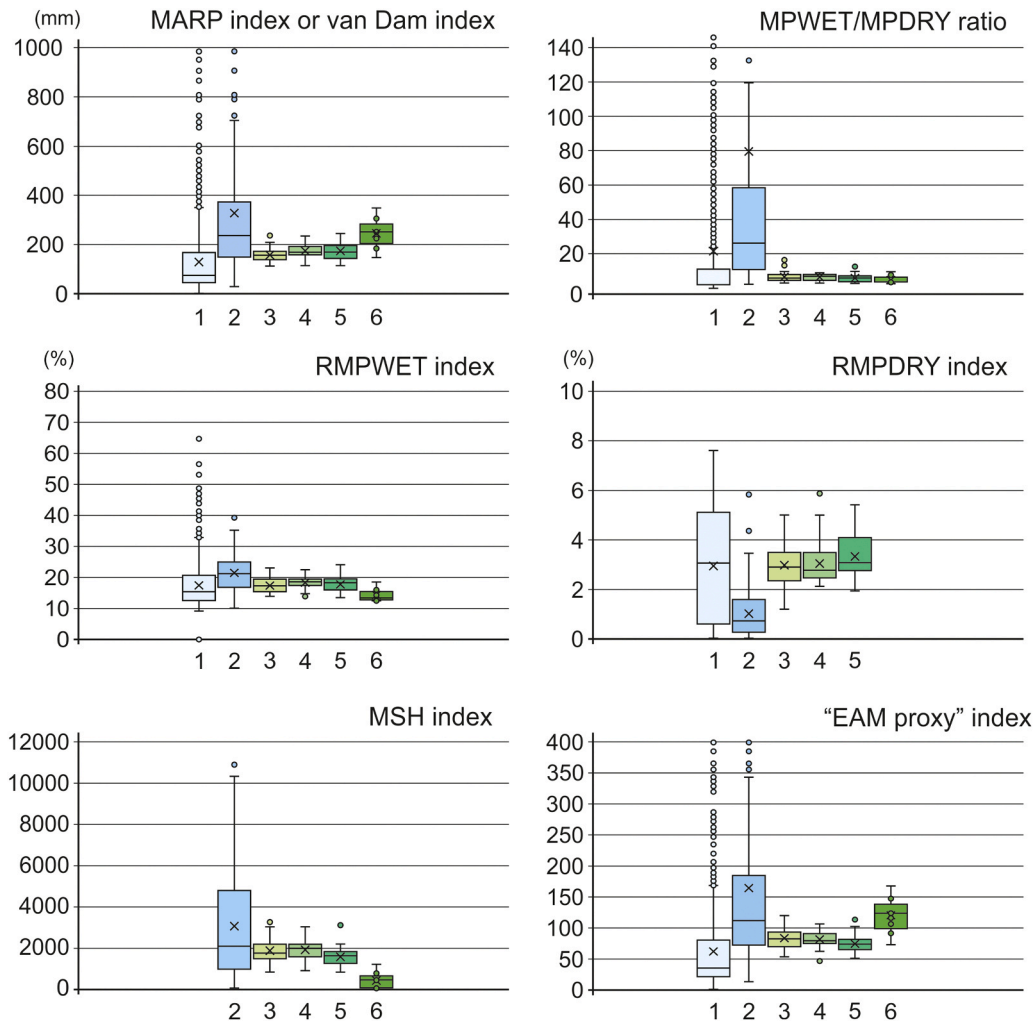

Fig. 11. Box plots for the variables and indices presently used to estimate monsoonal signals: 1 – modern (monsoon and non-monsoon) station data from Müller and Hennings (2000) in the global context, 2 – modern station data (Müller and Hennings, 2000) classified as monsoonal according to their Koeppen-Geiger climate types, 3 – late Eocene sites located in the realm of the extant East Asian Monsoon System (cf. Figs. 9), 4 – middle Eocene sites located in the realm of the extant East Asian Monsoon System, 5 – early Eocene sites located in the realm of the extant East Asian Monsoon System, 6 – Eocene sites located on the Indian Plate.

Table 2
Ranges of mean values of precipitation variables reconstructed and monsoon indices calculated for the Eocene sites of East Asia.

Precipitation variables, monsoon indices	MAPmean (mm)	MPWETmean (mm)	MPDRYmean (mm)	MARP or van Dam index (mm)	MPWET/ MPDRY ratio	RMPWET (%)	RMPDRY (%)	MSH	"EAMS proxy" index (this study)
late Eocene									
north of 50° N	1100–1250	173–230	30–59	115–192	3–8	14.0–19.3	2.5–5.2	738–2028	53–91
40–50° N	1158–1596	165–264	24–59	110–223	3–10	13.9–23.0	2.0–5.0	679–2504	52–104
south of 40° N	705–1286	116–245	10–48	90–201	4–16	12.9–20.1	1.2–3.5	870–3268	45–95
Indian Plate	1428–3141	265–389	51–101	218–349	4–13	12.4–18.5	1.3–3.7	74–3408	108–168
middle Eocene									
north of 50° N	1029–1422	147–247	34–61	86–232	2–7	11.8–21.4	2.2–5.3	553–2120	43–104
40–50° N	973–1357	161–250	25–59	114–235	3–9	14.0–21.7	2.1–5.9	1408–2432	47–106
south of 40° N	800–1650	151–320	27–56	119–287	4–11	13.9–22.5	2.1–4.2	921–3039	54–136
Indian Plate	—	—	—	—	—	—	—	—	—
early Eocene									
north of 50° N	1006–1555	165–291	27–59	126–238	3–9	13.4–20.7	2.0–5.1	1273–4313	59–111
40–50° N	803–1352	158–265	16–61	112–238	3–12	14.0–24.1	1.9–5.4	961–3116	51–114
south of 40° N	874–1130	145–196	26–59	118–185	4–7	14.8–20.2	2.8–4.8	514–2047	58–116
Indian Plate	1774–2681	230–359	83–101	184–306	3–8	12.5–18.5	2.4–4.6	74–1223	73–147

as is shown by increasing values in the north and south, but decreasing values in the middle and eastern parts of central China (Quan et al., 2012a). Our data indicate very high values of MAP varying from 900 to 1100 mm in the early Eocene and from 700 to 1200 mm in late Eocene. Moreover, according to our data, a "drier" zone established and became larger during the middle and late Eocene, extending westward to ~80° E.

Regarding the lower latitudes, our present reconstruction shows, in

addition to two moderate humid subtropical subzones distinguished by Bondarenko and Utescher (2024), the presence of a very humid zone (with high MAP at 1600–2600 mm) in the tropics, based on palaeosites from India located in the early Eocene near the equator. Shukla et al. (2014) also suggest high MAP of ~1800 mm for the early Eocene of India, based on CLAMP analysis. Recent studies on the middle and late Eocene floras of south China reveal humid subtropical conditions, with CLAMP-based estimates being in the order of the presently reconstructed early Eocene data (~2000 mm and higher; Jin et al., 2017).

There are no significant changes for mean values of MPWET in time, but there are spatial patterns during the Eocene (Fig. 3, Table 2). High Arctic was much wetter than the present, especially in the early Eocene, and declining thereafter. Continental interior mid-latitudes were much wetter than the present and again wettest in the early Eocene. The eastern part of the mid-latitudes (e.g. Primorye, Sakhalin) was wetter than the present, and becoming wetter towards the late Eocene. The south China was drier than present, but becoming wetter since the middle Eocene. The Indian Plate was very wet, also W India which was much wetter than present. Comparable patterns are obtained for MPDRY (Fig. 4).

Generally, our data show higher levels of MAP, MPdry and MPwet for the high and higher mid-latitudes of the eastern part of Eurasia in the Eocene compared to the present-day. This correlates well with higher temperature values (MAT, CMMT, and WMMT), as well as with a latitudinal temperature gradient of the Pacific side of Eurasia in the early Eocene, being about only one third of the present (Wolfe, 1978; Greenwood and Wing, 1995) or even lesser, as suggested by the Pacific data (Bondarenko and Utescher, 2022). Higher temperatures lead to a higher moisture content of the atmosphere and higher evaporation, resulting in higher levels of precipitation. As seen, the fossil data do not plot in the core area of monsoon stations (Fig. 5).

5.2. *Precipitation seasonality – which seasonality is monsoonal?*

In high and mid-latitudes, the modern climate of eastern Eurasia is characterized by pronounced temperature and precipitation seasonality. The seasonal contrast of temperature today increases to the north, while precipitation seasonality, on the contrary, decreases to the north. The modern spatial pattern of MARP over Eurasia, as illustration of precipitation seasonality, is shown in Fig. 6. The Eocene MARP was significantly higher-than-present in the mid-latitudinal intra-continental parts, including the region of the modern Tibetan Plateau. This concerns regions in which today, overall dry conditions prevail. In the continental area presently under the influence of the EAM, Eocene MARP tended to be significantly lower compared to present-day. The reconstructed relatively high past MPWET level coupled with distinctly higher-than-present MPDRY indicate that, during the Eocene, the climate of eastern Eurasia in general was more humid compared to today. This is in good agreement with the reconstructed high MAP level. Our reconstructions show a clear division into three zones: a moderately wet zone north of ca. 50° N, a moderately dry zone south of ca. 50° N, and a very humid zone south of ca. 10–15° N (Fig. 2, Table 2). It is interesting to note that under the existence of a clear zonation based on precipitation variables, the Eocene MARP values are similar across the studied sector, i.e., do not show the distinct pattern evident from modern data. Nevertheless, based on MARP values, High Arctic and continental interior north of 50° N were much wetter than present in the early Eocene, but are declining thereafter. Mid-latitudes of the Pacific coast were mainly drier than present, but trend to high MARP in some localities in the middle Eocene. The southern part of the continental interior was mainly wetter that present throughout Eocene. South China trended to higher MARP since the middle Eocene. A similar pattern was noted for the early Paleogene of East Asia (Bondarenko and Utescher, 2024). According to Jacques et al. (2013), MARP and the van Dam index only map the seasonality in precipitation, but do not consider the distribution of the precipitation throughout the year. Therefore, high index values are also retrieved for regions with high winter precipitation, but low summer precipitation, even if the climate is non-monsoonal.

The MPWET/MPDRY ratio has been used in literature as another parameter to describe seasonality of precipitation and potential presence of monsoon climate. According to Lau and Yang (1997) and Zhang and Wang (2008), ratios exceeding 6:1 are considered indicative of a monsoonal regime. Generally, all our localities are characterized by a marked difference in the MPWET/MPDRY ratio, which mainly varies from 3:1–8:1, but for some floras even from 10:1–16:1 (Appendix 3). The lowest ratio is calculated for the middle Eocene, the highest – late Eocene (Tables 2 and 3). A pronounced seasonality of precipitation was suggested by many researchers for the late Cretaceous and early Cenozoic. In the early Eocene of northern Yakutia (Eastern Siberia) the MPWET/MPDRY ratio varied from 3:1–9:1 in Lena River Delta (Bondarenko et al., 2022), and from 3:1–5:1 at Tastakh Lake (Bondarenko and Utescher, 2023). According to Bondarenko et al. (2020a), the pronounced seasonality of precipitation of the Paleogene climate of Primorye gradually increased from ca. 5:1–7:1 in the early Palaeocene to ca. 4:1–9:1 in the late Oligocene. According to Quan et al. (2012b), seasonal variability in precipitation in the early Paleogene of northeastern China appears to occur in most sites. An essentially "summer wet" (3:1) climate has been proposed for the Arctic in the Eocene based on isotopic analysis of fossil wood interpreted to have been evergreen (Schubert et al., 2012), but an "ever wet" precipitation regime for this epoch is indicated by leaf form based on predominantly deciduous angiosperm taxa (West et al., 2015). According to Bondarenko and Utescher (2024), all localities of East Asia in the early Paleogene are characterized by a marked difference in the MPWET/MPDRY ratio, which mainly varies from 3:1–8:1, but for some macrofloras even from 10:1–15:1. Shukla et al. (2014) indicated a 3WET/3DRY ratio from 9:1–12:1 for the early Eocene of India. Such a large range can most likely be explained by taphonomic effect, topography, distance from the sea/ocean, and local conditions, because there is no regularity in spatial distribution of the ratios. For comparison, the MPWET/MPDRY ratios were calculated based on modern climatic data. The present-day ratio ranges from 2:1–242:1 (Appendix 6). Moreover, there is also no regularity in spatial distribution of the ratio and the highest values (anomalies) do not coincide with the EAMS area. So, the high precipitation seasonality is not necessarily indicative for monsoon climate, especially at high and mid-latitudes, where seasonality can result from other mechanisms (e.g., mid-latitude storm tracks, polar front migration, etc.).

The indices RMPWET and RMPDRY are widely used for estimation of monsoon intensity in reconstructions based on the palaeobotanical record (Jacques et al., 2014; Shukla et al., 2014; Spicer et al., 2014; West et al., 2015). According to Jacques et al. (2011a,b), the ratios are a good indication of past monsoon intensity (winter and summer, respectively). According to Zhang and Wang (2008), regions that exhibit monsoons, or "monsoon-type" precipitation during summer are not seasonally equable, i.e. characterized by RMPWET exceeding 55 % for the wet season. The Eocene RMPWET varies from 11.8 % to 24.1 % (Table 2). In the early Paleogene of the eastern Eurasia, the calculated RMPWET values at high latitudes range from 12.5 % to 18.1 %, while at low – from 13.3 % to 24.1 % (Bondarenko and Utescher, 2024). Such distribution of RMPWET suggests a more pronounced seasonality of precipitation at high latitudes and a less pronounced seasonality of precipitation in the mid- and low latitudes. Similar patterns are obtained for the Eocene of East Asia. The present-day RMPWET varies from 12.1 % to 41.5 % for meteo stations characterized by monsoon and non-monsoonal climate according to the Koeppen – Geiger classification. The modern meteo station Surat (21°20′ N, 72°83′ E) with RMPWET 41.5 % is close to the palaeosite Vastan (21°25′ N, 73°07′ E) with the early Eocene RMPWET 14.3 % (Appendix 6). Therefore, RMPWET values calculated from our record cannot be interpreted in terms of a monsoonal type of climate (summer monsoon). Moreover, at high latitude, the revealed precipitation seasonality is not necessarily indicative of a monsoonal climate (for more details cf. Bondarenko and

Table 3
Comparison of all monsoon indices applied performing under different settings (high-latitude vs. tropical sites).

Monsoon index	MARP or van Dam index (mm)	MPWET/MPDRY ratio	RMPWET (%)	RMPDRY (%)	MSH	"this study" index
modern non-monsoon						
high latitudes	22–153	2–6	10.2–16.9	2.5–6.6	216–2374	11–76
low latitudes	0–952	2–245	0–64.7	0–7.6	0–5498	0–461
modern monsoon						
high latitudes	34–94	2–43	14.5–35.3	0.8–5.8	921–3610	15–44
low latitudes	90–1397	3–133	10.1–39.3	0–4.5	65–10897	42–643
late Eocene						
high latitudes	115–149	3–5	14.0–16.1	3.1–5.2	1256–2028	53–73
low latitudes	139–349	4–13	12.4–20.1	1.3–3.8	74–3408	66–168
middle Eocene						
high latitudes	104–232	3–7	12.5–21.4	3.2–5.3	1216–2120	52–104
low latitudes	156–287	4–11	13.9–22.5	2.1–4.2	921–2857	73–136
early Eocene						
high latitudes	126–206	3–9	14.8–20.2	2.0–5.1	1273–4313	59–101
low latitudes	130–306	3–8	12.5–20.1	2.4–4.5	74–2047	62–148

Note: high latitudes – north of 60° N, low latitudes – south of 30° N.

Utescher (2019) and discussions therein), but can be explained by an enhanced hydrological cycle during the Arctic summers supposed to cause high precipitation and humidity, under the presence of a permanent polar cloud cap (Spicer and Herman, 2010; Eldrett et al., 2014). The Eocene pattern of the southern part of East Asia (mid- and low latitudes) was possibly related to an early established monsoon-type circulation over East Asia (Quan et al., 2011, 2012a; Shukla et al., 2014) and enhanced flow of humid air masses from the Pacific to inland areas of the northeast Asia. Li et al. (2022) indicate that evolution and distribution of vegetation in East Asia during the Eocene, with the global cooling, were triggered by monsoonal intensity, rain-shadow effects of the central and southwestern China highlands and basin extensions in the Pacific coastal realm to the east. According to Spicer et al. (2017), monsoonal climates at low latitudes (<32° N) in the early Eocene strongly depended on seasonal latitudinal migrations of the Intertropical Convergence Zone (ITCZ), continental configuration, orography and the strength of Hadley circulation. Based on our reconstructions (Fig. 7), the highest values of RMPWET during the Eocene do not exceed 25 % even at mid- and low latitudes and, vary within a narrow range and are evenly distributed over the study area (i.e., do not show any latitudinal or meridional gradients). It can be assumed that our record cannot be interpreted unambiguously in terms of a monsoonal type of climate. As noted by Spicer et al. (2016), precipitation patterns are strongly influenced by factors other than those associated with the monsoon circulation, particularly at low latitudes such as southern China. Here, any changes in the seasonal latitudinal migration of the ITCZ, driven for example by changes in the latitudinal temperature gradient (Hasegawa et al., 2012), will affect the precipitation seasonality at any given palaeosite. Indices based on such seasonality should therefore be treated with caution at low latitudes, which makes it particularly difficult to detect the onset or change in the intensity of the topographically modified monsoon circulation – a critical issue for understanding the drivers of the EAMS.

The Eocene RMPDRY varies from 1.2 % to 5.9 %. Based on data of Bondarenko and Utescher (2024), in the early Paleogene of the eastern Eurasia, at high latitudes, the RMPDRY ranges from 2.5 % to 5.1 %, while at low – from 2.9 % to 4.8 %. Similar patterns are obtained for the Eocene of East Asia. The present-day RMPDRY varies from 0 % to 5.8 % for meteo stations characterized by monsoon and non-monsoonal climate according to the Koeppen – Geiger classification. Moreover, the modern meteo station Lhasa (29°67′ N, 91°12′ E) with RMPDRY 0 % is close to the palaeosite Xigaze (29°30′ N, 88°90′ E) with the early Eocene RMPDRY 2.5 % (Appendix 6). Based on our reconstructions (Fig. 8, Tables 2 and 3), the values of RMPDRY during the Eocene vary within a narrow range and are evenly distributed over the study area (i.e., do not show any latitudinal or meridional gradients). Therefore, it can be assumed that our record cannot be interpreted unambiguously in terms of a monsoonal type of climate (winter monsoon).

High values of the MSH index, according to Liu et al. (2011), point to a comparatively strong monsoonal regime, but our calculations obviously have a reverse result (Tables 2 and 3). The lowest MSH values for the Eocene of East Asia are obtained for early Eocene microfloras in India, while the highest values are characteristic for early Eocene microfloras at high latitudes. Also, in the case of the MSH, there is no clear regularity in the spatial distribution over East Asia. According to Jacques et al. (2013), the Liu et al. index values are high for eastern Asia, and high latitudes of the Northern Hemisphere. However, values for all other regions, including India, are low. This index uses the differences in the precipitations between the driest and warmest months. However, in tropical regions, the warmest month usually is not in the time-span of monsoonal rainfall, but in the dry season. Therefore, this index overlooks the seasonality in precipitation in intertropical regions (Jacques et al., 2013).

The modern spatial pattern of the presently introduced monsoon "EAM proxy" (Fig. 9) is in good agreement with the area of modern monsoon distribution in East Asia. A similar spatial pattern shows MARP. However, the Eocene patterns are fundamentally different from the modern one and show no anomalies (Fig. 10). The threshold of the proxy should exceed ~ 47 to be indicative for monsoonal climate (see Section 3.3). Most of the floras have "EAM proxy" values in range from 54 to 94 (in the early Eocene – 70 floras (84.3 %), in the middle Eocene – 65 floras (78.3 %), and in the late Eocene – 56 floras (76.7 %)). A minor proportion of floras has "EAM proxy" values in range from 95 to 129 (in the early Eocene – 11 floras (13.2 %), in the middle Eocene – 10 floras (12.0 %), and in the late Eocene – 9 floras (12.3 %)). Spatial patterns of these floras show wide and equal distribution during the Eocene (Tables 2 and 3). The floras with higher values of the "EAM proxy" are located in low latitudes that can be explained by high precipitation seasonality caused by changes in the seasonal latitudinal migration of the ITCZ. A number of authors (Charney, 1969; Sikka and Gadgil, 1980; Chao and Chen, 2001; Gadgil, 2003; Wang, 2009) also explain the monsoon by influence of the ITCZ.

As can be seen from Table 1, the minimum Eocene values obtained for the monsoon indices presently considered largely overlap with modern values from monsoonal type climate stations. Due to the overlapping data ranges, the min, max, and mean values may be less meaningful. Therefore, to better reflect the underlying data structure, boxplots are shown for individual variables considering modern monsoon stations (Müller and Hennings, 2000) and, data obtained for early, middle, and late Eocene sites located in the realm of the extant EAM and those on the Indian Plate (Fig. 11). As can be seen from Fig. 11, index values calculated for modern meteorological stations characterized by the corresponding type of the modern climate (both monsoon and non-monsoon) in the global context (1) or monsoon (2) climate

according to the Koeppen–Geiger classification have overlapping areas. The indices values calculated for the late (3), middle (4) and early (5) Eocene sites of East Asia are mainly at the low end of the 50 %ile boxes obtained for modern monsoonal stations, or slightly below. However, the MPWET/MPDRY ratio is clearly lower than the modern core data, and RMPDRY is significantly exceeding present-day values. Thus, our data suggest a weak or absent summer monsoon for this region which coincides with the results of the PCA (Fig. 5). Moreover, RMPDRY data clearly indicate the absence of a winter monsoon and, accordingly, suggest a weak or absent Siberian High throughout the Eocene. The Eocene values of the presently proposed "EAM proxy" and MSH suggest a strengthening of the monsoon from the early (5) to the late (3) Eocene (Fig. 11). For Eocene sites located on the Indian Plate (6), the indices considered here lead to ambiguous solutions. While MARP and our "EAM proxy" clearly indicate the presence of a monsoon in the Eocene, MPWET/MPDRY ratio, MSH and RMPWET point to its absence, but may work less reliably with tropical monsoon climates.

Given the complexity of the physical processes behind monsoonal circulation, indices and proxies based on few precipitation variables, as they are available e.g. in CA reconstructions from the palaeobotanical record, have to be regarded as relatively crude proxies for monsoon intensity. This also holds for the "EAM proxy" presently introduced. Nevertheless, the index performs well in the modern EAMS region, where it can be statistically tested using present-day climatological data (WORLDCLIM) and the published outline of the monsoonal region. Further tests in other regions will be necessary, but for that purpose, additional data on modern monsoon reach and intensity at the global scale would be required.

5.3. Planetary circulation or monsoon?

For the Eocene of the eastern Eurasia, our reconstruction reveals fundamentally different precipitation pattern compared to present (see Section 5.1). It shows a clear subdivision into three zones. Between the moderate wetter and drier zones, within the range of ca. 5° to south and north from 50° N, a transition zone can be distinguished where both, sites with higher and lower MAP values are observed (Fig. 2, Table 2). The asymmetric (NW-SE) orientation of these zones is mirrored the northward energy transport by ocean and atmosphere. A similar pattern was also reported for temperature (Bondarenko and Utescher, 2022) and precipitation parameters (Bondarenko and Utescher, 2024) reconstructed for the early Paleogene. This pattern more points to a planetary circulation and not so much toward monsoonal conditions. Our data suggest that, during the Eocene, the global atmospheric circulation consisted of two well-defined cells, Hadley and Ferrell, while the polar cell was either absent or located over the Arctic Ocean and was very weak. This would explain the presence of a drier zone to the south and a wetter zone to the north. On the other hand, as objected by Quan et al. (2012a), if the central China had been dominated by subtropical highs caused by the sinking of hot and dry air from the Eocene Hadley cell, it should have been largely year-round arid and with low primary productivity, as observed in the modern deserts and steppes at the Horse latitude (Rohli and Vega, 2008). Therefore, we speculate that, due to the overall higher humidity level of the atmosphere under the distinctly raised Eocene temperatures and the reduced extent of continental area and coeval presence of additional moisture sources such as epicontinental seas to the west, a year-round arid and desert zone did not form. In addition, it is possible that the weak Eocene temperature gradient (Bondarenko and Utescher, 2022) may have further mitigated, the Hadley and Farrell cells.

It seems that the boundary between the Hadley and Farrell cells ran at about 50° N, while the transition zone may reflect the region of shorter-term migration/shifting of these cells (cf. Bondarenko and Utescher, 2022). Comparable conditions of a very humid and warm Arctic may have already existed during the early Late Cretaceous (Spicer et al., 2019). According to Spicer et al. (2019), it is likely that at that time, the polar front was more diffuse and displaced towards the pole in comparison to present, while a warm Arctic Ocean is considered a key component of a then weaker polar high. Moreover, it should be noted that, in the early Eocene, the drier zone was quite narrow, extending to ~100 E. This may have corresponded to the limit of the western humidity transfer. However, starting from the middle Eocene and continued in the late Eocene, the drier zone became broader, then extending to ~80° E (Fig. 2). What could have influenced it? Of the major events at this time, there was a collision of India and Eurasia, which led to the formation of a large-scale change in landscape. This could have due to the retreat of the Paratethys Sea and strengthened the western transfer.

A main feature of the EAM is a dry cold season. The winter monsoon deeply penetrates into eastern Asia supported by a strong Siberian High (Molnar et al., 2010; Spicer et al., 2016). Today, the Siberian High is a massive of cold dry air accumulating in the northeast of Eurasia from September until April. Its greatest size and strength is reached in winter, with air temperatures below −40 °C in the center of the high-pressure area (Dando, 2005). Boos and Kuang (2010), (2013) and Wu et al. (2007), (2012) show that the East Asian summer monsoon (EASM) is in any case temperature-controlled. According to Bondarenko and Utescher (2022), even the lowest values of the lower limits of the CIs for CMMTs in the early Eocene over eastern Eurasia did not fall below −3.0 °C. Moreover, the Paleogene palaeogeographic configuration of Asia fundamentally differed from modern (Scotese, 2013). The Tarim area and Siberian Platform were covered by a shallow epicontinental sea (Volkova and Kuz'mina, 2005; Z. Zhang et al., 2007, 2012; Bosboom et al., 2014, 2015) that reduced the width in latitude of the continental area by about one quarter compared to present. During the early Paleogene, the maximum extent of marine transgression occurred in the mid-latitudes of the central Eurasia, with over 60 % of the West Siberian Plate covered by water (Volkova and Kuz'mina, 2005; Akhmetiev et al., 2012). Thus, it is most likely that the Siberian High, as one of the main drivers of the EAM, did not yet exist in the Eocene, at least not as a permanent feature.

When relying on monsoon indices based on climate variables derived from fossil floras it has to be considered that there are various other factors that strongly influence precipitation patterns, especially at low latitudes. Among these factors, Spicer et al. (2019) cite changes in the seasonal latitudinal migration of the ITCZ due to changes in the latitudinal temperature gradient. Therefore, monsoon indices should be used with caution. Another factor that may make it difficult to use rainfall patterns as an indicator of past monsoon intensity is the fact that most palaeobotanical records are preserved in basins where precipitation is commonly not the only source for humidity. This may introduce a bias towards humid conditions in palaeoclimate reconstructions (Spicer et al., 2019).

Leaf architectural signatures revealed that the Eocene EAM in the southern China is primarily driven by the wider seasonal migrations of the ITCZ (Spicer et al., 2016, 2017; Spicer, 2017; Herman et al., 2017). If this is simply a reflection of wider ITCZ zonal migrations under a shallower equator-to-pole thermal gradient in the Eocene greenhouse conditions (Greenwood and Wing, 1995; Huber and Goldner, 2012), then the southern China should have been subject to the effects of ITCZ seasonal migration prior to the middle Eocene, such as the extremely warm interval of the early Eocene (Xie et al., 2019). Consistent with geological evidence, numerical simulations also found that monsoon climates were restricted to the southern-most Hainan Island during the Paleocene to early Eocene, and that these tropical monsoons mainly resulted from the seasonal migrations of the ITCZ (Guo et al., 2008; Liu et al., 2015). The existence of ITCZ monsoons across the southern Asia (south of 20° N) can be traced back to very early geological history (Guo et al., 2008; Liu et al., 2015), but the monsoons becoming established in subtropical China (20–25° N) during the middle Eocene are conceptually different from the tropical monsoons in low latitudes, and would have been controlled by other factors (Xie et al., 2019).

As regards the timing of the initiation of monsoon systems in the east and southeast Asia, various authors suggest that the SAM existed as early as Eocene (Licht et al., 2014; Shukla et al., 2014; Spicer et al., 2016; Bhatia et al., 2021). More recent studies indicate that the palaeomonsoon in East Asia may have initiated at lower latitudes, also in the course of the Eocene as is evident from coal and oil shale deposits along the southern margins of the subtropical arid zone (Spicer et al. 2016, 2020 for a summary). Also, Li et al. (2022) relate changes in the spatial distribution of Eocene vegetation in East Asia to the influence of a monsoonal climate. As causes for the EAM initiation during the Eocene, enlargement of the continental area as a result of the Indo-Eurasia collision and uplifting of blocks in the realm of the present-day Tibetan Plateau can be cited (An et al., 2015). Also, increased continentality of the climate related to the step-wise retreat of the Paratethys from the Tarim Basin since the middle Eocene (Bosboom et al., 2011) may have contributed to the initiation of the EASM. Summarizing these facts and according to the present results obtained we assume that the EAM did not yet exist or was very weak in the earlier part of the Paleogene and probably started to evolve at lower latitudes as EASM during the middle to late Eocene.

6. Conclusions

1) The Eocene precipitation patterns of eastern Eurasia fundamentally differed from the modern ones. Our reconstruction reveals that at high and mid-latitudes MAP was significantly higher than present during the Eocene. Moreover, our reconstruction reveals a distinct zonal pattern persisting throughout the Eocene. In total, three different zones are deciphered: a moderately wet zone north of ca. 50° N, a moderately dry zone south of ca. 50° N, and a very humid zone south of 10–15° N.
2) The global atmospheric circulation during the Eocene fundamentally different from the modern one. Our data suggest that the global atmospheric circulation consisted of two well-defined cells, Hadley and Ferrell, while the polar cell was either absent or very weak, possibly located over the Arctic Ocean. The boundary between the Hadley and Farrell cells ran at about 50° N, while data from sites located near the transition zone point to shorter-term migrations/shifts of the boundary during the Eocene. Due to the overall higher-than-present humidity and the reduced size of the continental interior, but the presence of additional moisture sources such as epicontinental seas to the west of the study area, a year-round arid desert zone did not form. Moreover, it can be assumed that the shallow temperature gradients reconstructed for the Eocene caused weaker-than-present Hadley and Farrell cells.
3) The monsoon indices and proxies considered here lead to ambiguous evidences regarding the presence of monsoon circulation in the study area during the Eocene. Our data mostly suggest a weak or absent summer monsoon which coincides with the results of the performed PCA placing Eocene data in modern climate space. The RMPDRY data calculated from our floral record clearly indicate the absence of a winter monsoon and, hence, suggest a weak or absent Siberian High throughout the Eocene. The values obtained for the presently proposed "EAM proxy" and the MSH index suggest a strengthening of the monsoon from the early to late Eocene. For Eocene sites located on the Indian Plate, MARP and "EAM proxy" clearly indicate monsoonal conditions, while MPWET/MPDRY ratio, MSH and RMPWET point to its absence, but may work less reliably with tropical monsoon climates, a problem that needs to be addressed in future research with an extended data set.
4) Given the complexity of the physical processes behind monsoonal circulation, monsoon indices based on few variables, as commonly available in deep time reconstructions, have to be regarded as relatively crude proxies for monsoon presence and intensity. It is shown that each index has its strengths and flaws, while the joint application of various different indices is useful although there are a couple of minor contradictions.

Declaration of Competing Interest

The authors declare that they have no known competing financial interests or personal relationships that could have appeared to influence the work reported in this paper.

Acknowledgements

The author is very grateful to Torsten Utescher for the invaluable assistance in the analysis and interpretation of the obtained data. The author is also thankful to Gaurav Srivastava and an anonymous reviewer for carefully revising the manuscript and for their constructive comments and valuable suggestions that substantially improve the manuscript. The research was carried out within the state assignment of Ministry of Science and Higher Education of the Russian Federation (theme No. 124012200182–1). This work is a contribution to NECLIME (the research Network on Cenozoic Climate and Ecosystems).

Appendix A. Supporting information

Supplementary data associated with this article can be found in the online version at doi:10.1016/j.hisbio.2025.100035.

Data availability

Data will be made available on request.

References

Akhmetiev, M.A., 2004. The paleocene and eocene global climate. paleobotanical evidences. In: Semikhatov, M.A., Chumakov, N.M. (Eds.), Climate in the Epoches of Major Biospheric Transformations (Trudy Geologicheskogo Instituta RAN, 550. Geologicheskii institute Rossiiskoi akademii nauk, pp. 10–43.

Akhmetiev, M.A., Zaporozhets, N.I., Benyamovskiy, V.N., Aleksandrova, G.A., Iakonleva, A.I., Oreshkina, T.V., 2012. The Paleogene history of the Western Siberian seaway – a connection of the Peri-Tethys to the Arctic Ocean. Austrian J. Earth Sci. 105 (1), 50–67.

Amon, E.O., 2001. Marine waters of the Ural region in the Middle and Late Cretaceous time. Geol. Geofiz 42 (3), 471–483.

Amon, E.O., 2018. Factors and conditions of accumulation of biogenic silicites in the Paleogene basin of Western Siberia. Bull. Moip. Dep. Geol. 93 (4), 51–67.

An, Z.S., Kutzbach, J.E., Prell, W.L., Porter, S.C., 2001. Evolution of Asian monsoons and phased uplift of the Himalayan – Tibetan plateau since late Miocene times. Nature 411, 62–66. https://doi.org/10.1038/35075035.

An, Z.S., Wu, G.X., Li, J.P., Sun, Y.B., Liu, Y., Zhou, W.J., Cai, Y.J., Duan, A.M., Li, L., Mao, J.G., Cheng, H., Shi, Z.G., Tan, L.C., Yan, H., Ao, H., Chang, H., Feng, J., 2015. Global monsoon dynamics and climate change. Ann. Rev. Earth Planet. Sci. 43, 29–77 https://doi.org/1146/annurev-earth-060313-054623.

Bhatia, H., Khan, M.A., Srivastava, G., Hazra, T., Spicer, R.A., Hazra, M., Mehrotra, R.C., Spicer, T.E.V., Bera, S., Roy, K., 2021. Late Cretaceous – Paleogene monsoon climate vis-à-vis movement of the Indian plate, and the birth of the south Asia monsoon. Gondwana Res 93, 89–100. https://doi.org/10.1016/j.gr.2021.01.010.

Bondarenko, O.V., Utescher, T., 2022. Early Paleogene continental temperature patterns and gradients over eastern Eurasia. J. Asian Earth Sci. 239, 105401. https://doi.org/10.1016/j.jseaes.2022.105401.

Bondarenko, O.V., Utescher, T., 2023. Late early to early middle Eocene climate and vegetation change at Tastakh Lake (northern Yakutia, Eastern Siberia). Palaeobiodiversity Palaeoenvironments 103 (2), 277–301. https://doi.org/10.1007/s12549-022-00530-6.

Bondarenko, O.V., Utescher, T., 2024. Early Paleogene precipitation patterns over East Asia: was there a monsoon after all? Palaeobiodiversity Palaeoenvironments 104, 1–28. https://doi.org/10.1007/s12549-023-00586-y.

Bondarenko, O.V., Blokhina, N.I., Utescher, T., 2019. Major plant biome changes in the Primorye Region (Far East of Russia) during the Paleogene. Bot. Pac. 8 (1), 3–18. https://doi.org/10.17581/bp.2019.08106.

Bondarenko, O.V., Blokhina, N.I., Mosbrugger, V., Utescher, T., 2020a. Paleogene climate dynamics in the Primorye Region, Far East of Russia, based on a Coexistence Approach analysis of palaeobotanical data. Palaeobiodiversity Palaeoenvironments 100 (1), 5–31. https://doi.org/10.1007/s12549-019-00377-4.

Bondarenko, O.V., Blokhina, N.I., Evstigneeva, T.A., Utescher, T., 2022. Short-term climate and vegetation dynamics in Delta Lena River (northern Yakutia, Eastern Siberia) during the early Eocene. Palaeoworld 31 (3), 521–541. https://doi.org/10.1016/j.palwor.2021.09.006.

Boos, W.R., Kuang, Z.-M., 2010. Dominant control of the South Asian monsoon by orographic insulation versus plateau heating. Nature 463, 218–222. https://doi.org/10.1038/nature08707.
Boos, W.R., Kuang, Z.-M., 2013. Sensitivity of the South Asian monsoon to elevated and non-elevated heating. Sci. Rep. 3, 1192. https://doi.org/10.1038/srep01192.
Bosboom, R., Mandic, O., Dupont-Nivet, G., Proust, J.N., Ormukov, C., Aminov, J., 2015. Late Eocene palaeogeography of the proto-Paratethys Sea in Central Asia (NW China, southern Kyrgyzstan and SW Tajikistan). In: Brunet, M.F., McCann, T., Sobel, E.R. (Eds.), Geological Evolution of Central Asian Basins and the Western Tien Shan Range. Special Publications, Geological Society, London, pp. 565–588. https://doi.org/10.1144/SP427.11.
Bosboom, R.E., Dupont-Nivet, G., Houben, A.J.P., Brinkhuis, H., Villa, G., Mandic, O., Stoica, M., Zachariasse, W.-J., Guo, Z., Li, C., 2011. Late Eocene sea retreat from the Tarim Basin (west China) and concomitant Asian paleoenvironmental change. Palaeogeogr. Palaeoclimatol. Palaeoecol. 299, 385–398. https://doi.org/10.1016/j.palaeo.2010.11.019.
Bosboom, R.E., Abels, H.A., Hoorn, C., van den Berg, B.C.J., Guo, Z., Dupont-Nivet, G., 2014b. Aridification in continental Asia after the Middle Eocene Climatic Optimum (MECO). Earth Planet. Sci. Lett. 389, 34–42. https://doi.org/10.1016/j.epsl.2013.12.014.
Bosboom, R.E., Dupont-Nivet, G., Grothe, A., Brinkhuis, H., Villa, G., Mandic, O., Stoica, M., Kouwenhoven, T., Huang, W.T., Yang, W., Guo, Z.J., 2014a. Timing, cause and impact of the late Eocene stepwise sea retreat from the Tarim Basin (west China). Palaeogeogr. Palaeoclimatol. Palaeoecol. 403, 101–118. https://doi.org/10.1016/j.palaeo.2014.03.035.
Bruch, A.A., Utescher, T., Mosbrugger, V., NECLIME members, 2011. Precipitation patterns in the Miocene of Central Europe and the development of continentality. Palaeogeogr. Palaeoclimatol. Palaeoecol. 304, 202–211. https://doi.org/10.1016/j.palaeo.2010.10.002.
Budantsev, L.Yu, 1999. The reconstruction of the Cenozoic climates in eastern-north Asia based on palaeobotanical data. Bot. Zh. 84 (10), 36–45.
Chao, W.C., Chen, B.D., 2001. The origin of monsoon. J. Atmos. Sci. 58, 3497–3507. https://doi.org/10.1175/1520-0469(2001)058<3497:TOOM>2.0.CO;2.
Cohen, K.M., Harper, D.A.T., Gibbard, P.L., 2020. ICS International Chronostratigraphic Chart 2020/03. International Commission on Stratigraphy, IUGS ⟨www.stratigraphy⟩. org (accessed 23 December 2020).
van Dam, J.A., 2006. Geographic and temporal patterns in the late Neogene (12–3 Ma) aridification of Europe: The use of small mammals as paleoprecipitation proxies. Palaeogeogr. Palaeoclimatol. Palaeoecol. 238, 190–218. https://doi.org/10.1016/j.palaeo.2006.03.025.
Charney, J.G., 1969. The intertropical convergence zone and the Hadley circulation of the atmosphere. In: Proceedings of theWMO/IUGG Symposium on Numerical Weather Prediction in Tokyo. Jpn. Meteorol. Agency, Tokyo, pp. 73–79. Nov. 26–Dec. 4.
Dando, W.A., 2005. Asia. climates of Siberia, Central and East Asia. In: Oliver, J.E. (Ed.), Encyclopedia of World Climatology. Springer, Dordrecht, pp. 102–114. https://doi.org/10.1007/1-4020-3266-8.
Dupont-Nivet, G., Hoorn, C., Konert, M., 2008. Tibetan uplift prior to the Eocene-Oligocene climate transition: evidence from pollen analysis of the Xining basin transition. Geology (6), 987–990. https://doi.org/10.1130/0091-7613-37.6.506.
Eldrett, J.S., Greenwood, D.R., Polling, M., Brinkhuis, H., Sluijs, A., 2014. A seasonality trigger for carbon injection at the Paleocene–Eocene thermal maximum. Clim 10, 1–11. https://doi.org/10.5194/CP-10-759-2014.
Farnsworth, A., Lunt, D.J., Robinson, S.A., Valdes, P.J., Roberts, W.H.G., Clift, P.D., Markwick, P., Su, T., Wrobel, N., Bragg, F., Kelland, S.-J., Pancost, R.D., 2019. Past East Asia monsoon evolution controlled by paleogeography, not CO_2. Sci. Adv. 5, eaas1697. https://doi.org/10.1126/sciadv.aax1697.
Gadgil, S., 2003. The Indian monsoon and its variability. Ann. Rev. Earth Planet. Sci. 31, 429–467. https://doi.org/10.1146/annurev.earth.31.100901.141251.
Gladenkov, Yu.B., Bazhenova, OK, Grechin, V.I., Margulis, L.S., Salnikov, BA., 2002. The Cenozoic Geology and the Oil and Gas Presence in Sakhalin. GEOS, Moscow.
Gladenkov, Yu.B., Sinel'nikova, V.N., Chelebaeva, A.I., Shantser, A.E., 2005. Biosphere – Ecosystem – Biota in the Earth Past. The North Pacific Cenozoic ecosystems: Eocene – Oligocene of West Kamchatka and adjacent regions (To the centenary of Academician V.V. Menner). Transactions of the Geological Institute, Vol. 540. GEOS, Moscow.
Greenwood, D.R., Wing, S.L., 1995. Eocene continental climates and latitudinal temperature gradients. Geology 23, 1044–1048. https://doi.org/10.1130/0091-7613(1995).
Greenwood, D.R., Basinger, J.F., Smith, R.Y., 2010. How wet was the Arctic Eocene rain forest? Estimates of precipitation from Paleogene Arctic macrofloras. Geology 38, 15–18. https://doi.org/10.1130/G30218.1.
Grinenko, O.V., Sergeenko, A.I., Belolubskiy, I.N., 1997. Stratigraphy of the Paleogene and Neogene deposits of the North-East of Russia. Otechestvennaya Geol. 8, 14–20.
Guo, Z., Ruddiman, W.F., Hao, Q.Z., Wu, H.B., Qian, Y.S., Zhu, R.X., Peng, S.Z., Wei, J.J., Yuan, B.Y., Liu, T.S., 2002. Onset of Asian desertification by 22 Myr ago inferred from loess deposits in China. Nature 416, 159–163. https://doi.org/10.1038/416159a.
Guo, Z.-T., Sun, B., Zhang, Z.-S., Peng, S.-Z., Xiao, G.-Q., Ge, J.-Y., Hao, Q.-Z., Qiao, Y.-S., Liang, M.-Y., Liu, J.-F., Yin, Q.-Z., Wei, J.-J., 2008. A major reorganization of Asian climate by the early Miocene. Clim 4, 153–174. https://doi.org/10.5194/cp-4-153-2008.
Hasegawa, H., Tada, R., Jiang, X., Suganuma, Y., Imsamut, S., Charusiri, P., Ichinnorov, N., Khand, Y., 2012. Drastic shrinking of the Hadley circulation during the mid- cretaceous supergreenhouse. Clim 8, 1323–1337. https://doi.org/10.5194/cp-8-1323-2012.
He, C.X., Tao, J.R., 1997. A study on the Eocene flora in Yilan County, Heilongjiang. Acta Phytotax. Sin. 35, 249–256.
Herman, A.B., Spicer, R.A., Aleksandrova, G.N., Yang, J., Kodrul, T.M., Maslova, N.P., Spicer, T.E.V., Chen, G., Jin, J.-H., 2017. Eocene–early Oligocene climate and vegetation change in southern China: evidence from the Maoming Basin. Palaeogeogr. Palaeoclimatol. Palaeoecol. 429, 126–137. https://doi.org/10.1016/j.palaeo.2017.04.023.
Hijmans, R.J., Cameron, S.E., Parra, J.L., Jones, P.G., Jarvis, A., 2005. Very high resolution interpolated climate surfaces for global land areas. Int. J. Clim. 25, 1965–1978. https://doi.org/10.1002/joc.1276.
Huang, Q.H., Huang, F.T., Zhang, Y., Chen, C.R., Kong, H., Jin, X.X., 1998. New advance in the Tertiary strata study of the Tangyuan Rift. J. Stratigr. 22, 73–80.
Huber, B.T., Goldner, A., 2012. Eocene monsoons. J. Asian Earth Sci. 44, 3–23. https://doi.org/10.1016/j.jseaes.2011.09.014.
Huber, M., Caballero, R., 2011. The early Eocene equable climate problem revisited. Clim 7, 603–633. https://doi.org/10.5194/cpd-7-241-2011.
Jacques, F.M.B., Guo, S.X., Su, T., Xing, Y.-W., Huang, Y.-J., Liu, Y.S. (Ch), Ferguson, D. K., Zhou, Z.-K., 2011a. Quantitative reconstruction of the late Miocene monsoon climates of southwest China: a case study of the Lincang flora from Yunnan Province. Palaeogeogr. Palaeoclimatol. Palaeoecol. 304, 318–327. https://doi.org/10.1016/j.palaeo.2009.02.024.
Jacques, F.M.B., Su, T., Spicer, R.A., Xing, Y., Huang, Y., Wang, W., Zhou, Z., 2011b. Leaf physiognomy and climate: are monsoon systems different? Glob. Planet. Change 76, 56–62. https://doi.org/10.1016/j.gloplacha.2010.11.009.
Jacques, F.M.B., Su, T., Huang, Y.J., Wang, L., Zhou, Z.K., 2013. A global-scale test for monsoon indices used in palaeoclimatic reconstruction. Palaeoworld 22 (3–4), 93–100. https://doi.org/10.1016/j.palwor.2013.02.002.
Jacques, F.M.B., Su, T., Spicer, R.A., Xing, Y.-W., Huang, Y.-J., Zhou, Z.-K., 2014. Late Miocene southwestern Chinese floristic diversity shaped by the southeastern uplift of the Tibetan Plateau. Palaeogeogr. Palaeoclimatol. Palaeoecol. 411, 208–215. https://doi.org/10.1016/j.palaeo.2014.05.041.
Jin, J.H., Herman, A.B., Spicer, R.A., Kodrul, T.M., 2017. Palaeoclimate background of the diverse Eocene floras of South China. Sci. Bull. 62 (22), 1501–1503. https://doi.org/10.1016/j.scib.2017.11.002.
Kezina, T.V., 2005. Palynostratigraphy of coal deposits of the Late Cretaceous and Cenozoic of the Upper Amur River Region. Dal'nauka, Vladivostok.
Khan, M.A., Spicer, R.A., Bera, S., Gosh, R., Yang, J., Spicer, T.E.V., Guo, S., Su, T., Jacques, F.M.B., Grote, P.J., 2014. Miocene to Pleistocene floras and climate of the Eastern Himalayan Siwaliks, and new palaeoelevation estimates for the Namlinge–Oiyug Basin, Tibet. Glob. Planet. Change 113, 1–10. https://doi.org/10.1016/j.gloplacha.2013.12.003.
Lau, K.M., Yang, S., 1997. Climatology and interannual variability of the southeast Asian summer monsoon. Adv. Atmos. Sci. 14, 141–162. https://doi.org/10.1007/s00376-997-0016-y.
Li, Q.J., Utescher, T., Liu, Y.S. (Ch), Ferguson, D., Jia, H., Quan, C., 2022. Monsoonal climate of East Asia in Eocene times inferred from an analysis of plant functional types. Palaeogeogr. Palaeoclimatol. Palaeoecol. 601, 111–138. https://doi.org/10.1016/j.palaeo.2022.111138.
Li, Y.T., 1984. The Tertiary system of China. Geological Publishing House, Beijing.
Licht, A., van Cappelle, M., Abels, H.A., Ladant, J.B., Trabucho-Alexandre, J., France-Lanord, C., Donnadieu, Y., Vandenberghe, J., Rigaudier, T., Lecuyer, C., Terry, D., Adriaens, R., Boura, A., Guo, Z., Soe, A.N., Quade, J., Dupont-Nivet, G., Jaeger, J.J., 2014. Asian monsoons in a Late Eocene greenhouse world. Nature 513, 501–506. https://doi.org/10.1038/nature13704.
Liu, C., Shi, R., 2015. Boundary data of East Asia summer monsoon Geo_Eco_region (EASMBND)[J/DB/OL]. Digit. J. Glob. Change Data Repos. https://doi.org/10.3974/geobd.2015.01.12.V1.
Liu, J., Hertel, T.W., Diffenbaugh, N.S., Delgado, M.S., Ashfaq, M., 2015. Future property damage from flooding: sensetivity to economy and climate change. Clim. Change 132, 741–749. https://doi.org/10.1007/s10584-015-1478-z.
Liu, T.S., Zheng, M.P., Guo, Z.T., 1998. Initiation and evolution of the Asian monsoon system timely coupled with the ice-sheet growth and the tectonic movement in Asia. Quat. Sci. 3, 194–204.
Liu, X.D., Yin, Z.Y., 2002. Sensitivity of East Asian monsoon climate to the uplift of the Tibetan Plateau. Palaeogeogr. Palaeoclimatol. Palaeoecol. 183, 223–245. https://doi.org/10.1016/S0031-0182(01)00488-6.
Liu, Y.S.(C., Utescher, T., Zhou, Z.K., Sun, B.N., 2011. The evolution of Miocene climates in North China: preliminary results of quantitative reconstructions from plant fossil records. Palaeogeogr. Palaeoclimatol. Palaeoecol. 304, 308–317. https://doi.org/10.1016/j.palaeo.2010.07.004.
Meng, Q.T., Bruch, A.A., Sun, G., Liu, Z.J., Hu, F., Sun, P.C., 2018. Quantitative reconstruction of Middle and late Eocene paleoclimate based on palynological records from the Huadian Basin, northeastern China: evidence for monsoonal influence on oil shale formation. Palaeogeogr. Palaeoclimatol. Palaeoecol. 510, 63–77. https://doi.org/10.1016/j.palaeo.2017.11.036.
Miao, Y., Fang, X., Song, Z., Wu, F., Han, W., Dai, S., Song, C.H., 2008. Late Eocene Pollen Records and Palaeoenvironmental changes in Northern Tibetan Plateau. Science China Series D Earth Sci 51, 1089–1098. https://doi.org/10.1007/s11430-008-0091-7.
Molnar, P., Boos, W.R., Battisti, D.S., 2010. Orographic controls on climate and paleoclimate of Asia: thermal and mechanical roles for the Tibetan Plateau. Ann. Rev. Earth Planet. Sci. 38, 77–102. https://doi.org/10.1146/annurev-earth-040809-152456.
Mosbrugger, V., Utescher, T., 1997. The coexistence approach - a method for quantitative reconstructions of Tertiary terrestrial palaeoclimate data using plant fossils.

Palaeogeogr. Palaeoclimatol. Palaeoecol. 134, 61–86. https://doi.org/10.1016/S0031-0182(96)00154-X.
Mosbrugger, V., Utescher, T., Dilcher, D., 2005. Cenozoic continental climatic evolution of Central Europe. Proc. Natl. Acad. Sci. 102 (42), 14964–14969. https://doi.org/10.1073/pnas.0505267102.
Müller, M.J., Hennings, D., 2000. The Global Climate 592 Data Atlas on CD Rom. University Flensburg, Institute für Geografie, Flensburg.
Pavlyutkin, B.I., Petrenko, T.I., 2010. Stratigrafiya paleogen-neogenovykh otlozhenii Primor'ya. Dal'nauka, Vladivostok.
Pei, J., Sun, Z., Wang, X., Zhao, Y., Ge, X., Guo, X., Li, H., Si, J., 2009. Evidence for Tibetan Plateau uplift in Qaidam Basin before Eocene–Oligocene boundary and its climatic implications. J. Earth Sci. 20, 430–437. https://doi.org/10.1007/s12583-009-0035-y.
Quan, C., Liu, Y.C., Utescher, T., 2011. Paleogene evolution of precipitation in Northeastern China supporting the Middle Eocene intensification of the East Asian Monsoon. Palaios 26, 743–753. https://doi.org/10.2110/palo.2011.p11-019r.
Quan, C., Liu, (Y.S.) C., Utescher, T., 2012b. Paleogene temperature gradient, seasonal variation and climate evolution of northeast China. Palaeogeogr. Palaeoclimatol. Palaeoecol. 313–314, 150–161. https://doi.org/10.1016/j.palaeo.2011.10.016.
Quan, C., Liu, (Y.S.) C., Utescher, T., 2012a. Eocene monsoon prevalence over China: a palaeobotanical perspective. Palaeogeogr. Palaeoclimatol. Palaeoecol. 365–366, 302–311. https://doi.org/10.1016/j.palaeo.2012.09.035.
Quan, C., Liu, Z., Utescher, T., Jin, J.H., Shu, J.W., Li, Y.X., Liu, Y.S., 2014. Revisiting the Paleogene climate pattern of East Asia: a synthetic review. EarthSci. Rev. 139, 213–230. https://doi.org/10.1016/j.earscirev.2014.09.005.
Ramage, C.S., 1971. Monsoon meteorology (Int. Geophys. Ser, 15. Academic Press, California.
Rohli, R.V., Vega, A.J., 2008. Climatology. Jones and Bartlett Publishers, Sudbury, MA.
Schubert, B.A., Jahren, A.H., Eberle, J.J., Sternberg, L.S.L., Eberth, D.A., 2012. A summertime rainy season in the Arctic forests of the Eocene. Geology 40, 523–526. https://doi.org/10.1130/G32856.1.
Scotese, C.R., 2013. Map Folio 13, Early Eocene, Ypresian, 52.2 Ma), PALEOMAP PaleoAtlas for ArcGIS, volume 1, Cenozoic, PALEOMAP Project, Evanston, IL.
Shellito, C.J., Sloan, L.C., 2006. Reconstructing a lost Eocene paradise: Part I. Simulating the change in global floral distribution at the initial Eocene thermal maximum. Glob. Planet. Change 50, 1–17. https://doi.org/10.1016/j.gloplacha.2005.08.001.
Shi, F., Xin-rong, Z., Zhao-jun, L., He-yong, W., Jian-guo, Y., 2008. Thrust event of the provenances revealed by zircon fission track ages in Tangyuan Fault-Basin, NE China. Radiat. Meas. 43, S324–S328. https://doi.org/10.1016/j.radmeas.2008.04.079.
Shukla, A., Mehrotra, R.C., Spicer, R.A., Spicer, T.E.V., Kumar, M., 2014. Cool equatorial terrestrial temperatures and the South Asian monsoon in the Early Eocene: evidence from the Gurha Mine, Rajasthan, India. Palaeogeogr. Palaeoclimatol. Palaeoecol. 412, 187–198. https://doi.org/10.1016/j.palaeo.2014.08.004.
Sikka, D., Gadgil, S., 1980. On the maximum cloud zone and the ITCZ over Indian, longitudes during the southwest monsoon. Mon. Weather Rev. 108, 1840–1853. https://doi.org/10.1175/1520-0493(1980)108<1840:OTMCZA>2.0.CO;2.
Spicer, R.A., 2017. Tibet, the Himalaya, Asian monsoons and biodiversity – In what ways are they related? Plant Divers. 39 (5), 233–244. https://doi.org/10.1016/j.pld.2017.09.001.
Spicer, R.A., Herman, A.B., 2010. The late cretaceous environment of the arctic: a quantitative reassessment using plant fossils. Palaeogeogr. Palaeoclimatol. Palaeoecol. 295, 423–442. https://doi.org/10.1016/j.palaeo.2010.02.025.
Spicer, R.A., Herman, A.B., Liao, W.B., Spicer, T.E.V., Kodrul, T.M., Yang, J., Jin, J.H., 2014. Cool tropics in the middle Eocene: evidence from the Changchang flora, Hainan Island, China. Palaeogeogr. Palaeoclimatol. Palaeoecol. 412, 1–16. https://doi.org/10.1016/j.palaeo.2014.07.011.
Spicer, R.A., Yang, J., Herman, A.B., Kodrul, T., Maslova, N., Spicer, T.E.V., Aleksandrova, G.N., Jin, J.H., 2016. Asian Eocene monsoons as revealed by leaf architectural signatures. Earth Planet. Sci. Lett. 449, 61–68. https://doi.org/10.1016/j.epsl.2016.05.036.
Spicer, R.A., Yang, J., Herman, A., Kodrul, T., Aleksandrova, G., Maslova, N., Spicer, T.E.V., Ding, L., Xu, Q., Shukla, A., Srivastava, G., Mehrotra, R.C., Jin, J.H., 2017. Paleogene monsoons across India and South China: drivers of biotic change. Gondwana Res 49, 350–363. https://doi.org/10.1016/j.gr.2017.06.006.
Spicer, R.A., Valdes, P., Hughes, A., Yang, J., Spicer, T., Herman, A., Farnsworth, A., 2019. New insights into the thermal regime and hydrodynamics of the early Late Cretaceous Arctic. Geol. Mag. 157, 1729–1746. https://doi.org/10.1017/S0016756819000463.
Spicer, R.A., Su, T., Valdes, P.J., Farnsworth, A., Wu, F.X., Shi, G., Spicer, T.E.V., Zhou, Z. K., 2020. Why 'the uplift of the Tibetan Plateau' is a myth. Natl. Sci. Rev. 8 (1), nwaa091. https://doi.org/10.1093/nsr/nwaa091.
Srivastava, G., Spicer, R.A., Spicer, T.E.V., Yang, J., Kumar, M., Mehrotra, R.C., Mehrotra, N.C., 2012. Megaflora and palaeoclimate of a Late Oligocene tropical delta, Makum Coalfield, Assam: evidence for the early development of the South Asia Monsoon. Palaeogeogr. Palaeoclimatol. Palaeoecol. 342-343, 130–142. https://doi.org/10.1016/j.palaeo.2012.05.002.
Su, T., Xing, Y.W., Yang, Q.S., Zhou, Z.K., 2009. Reconstructions of mean annual temperature in Chinese Eocene Paleofloras based on leaf margin analysis. Acta Palaeontol. Sin. 48, 65–72.
Sun, J., Xiao, W., Windley, B.F., Ji, W., Fu, B., Wang, J., 2016. Provenance change of sediment input in the Northeastern Foreland of Pamir related to collision of the Indian Plate with the Kohistan – Ladakh Arc at Around 47 Ma. Tectonics 35, 315–338. https://doi.org/10.1002/2015TC003974.
Sun, X.J., Wang, P., 2005. How old is the Asian monsoon system? – palaeobotanical records from China. Palaeogeogr. Palaeoclimatol. Palaeoecol. 222, 181–222. https://doi.org/10.1016/j.palaeo.2005.03.005.
Tapponnier, P., Xu, Z., Roger, F., Meyer, B., Arnaud, N., et al., 2001. Oblique stepwise rise and growth of the Tibet Plateau. Science 294, 1671–1677. https://doi.org/10.1126/science.105978.
Utescher, T., Mosbrugger, V., 2007. Eocene vegetation patterns reconstructed from plant diversity – A global perspective. Palaeogeogr. Palaeoclimatol. Palaeoecol. 247, 243–271. https://doi.org/10.1016/j.palaeo.2006.10.022.
Utescher, T., Bruch, A.A., Micheels, A., Mosbrugger, V., Popova, S., 2011. Cenozoic climate gradients in Eurasia a palaeo-perspective on future climate change? Palaeogeogr. Palaeoclimatol. Palaeoecol. 304, 351–358. https://doi.org/10.1016/j.palaeo.2010.09.031.
Utescher, T., Bruch, A.A., Erdei, B., François, L., Ivanov, D., Jacques, F.M.B., Kern, A.K., Liu, (Y.-S.) C., Mosbrugger, V., Spicer, R.A., 2014. The Coexistence Approach – theoretical background and practical considerations of using plant fossils for climate 666 quantification. Palaeogeogr. Palaeoclimatol. Palaeoecol. 410, 58–73. https://doi.org/10.1016/j.palaeo.2014.05.031.
Utescher, T., Bruch, A., Mosbrugger, V., 2024. The Palaeoflora Database – Documentation and Data (Version 2024) [Data set]. Zenodo. https://doi.org/10.5281/zenodo.10881069.
Vasilieva, O.N., Levina, A.P., 2007. Organic-walled phytoplankton in the upper Cretaceous and Paleogene deposits of the Kushmurun section of the Turgai trough (Kazakhstan). Bull. Moip. Dep. Geol. 82 (2), 40–55.
Volkova, V.S., Kuz'mina, O.B., 2005. Flora, vegetation, and climate of the middle Cenophytic (Paleocene – Eocene) of Siberia. Geol. Geofiz 46 (8), 844–855.
Wang, C.S., Dai, J., Zhao, X., Li, Y., Graham, S.A., He, D., Ran, B., Meng, J., 2014. Outward-growth of the Tibetan Plateau during the Cenozoic: a review. Tectonophysics 621, 1–43. https://doi.org/10.1016/j.tecto.2014.01.036.
Wang, J., Wang, Y.J., Liu, Z.C., Li, J.Q., Xi, P., 1999. Cenozoic environmental evolution of the QaidamBasin and its implications for the uplift of the Tibetan Plateau and the drying of central Asia. Palaeogeogr. Palaeoclimatol. Palaeoecol. 152, 37–47. https://doi.org/10.1016/S0031-0182(99)00038-3.
Wang, P., 2009. Global monsoon in a geological perspective. Chin. Sci. Bull. 54, 1–24.
Wang, Q., Ferguson, D.K., Feng, G.P., Ablaev, A.G., Wang, Y.F., Yang, J., Li, Y.L., Li, C.S., 2010. Climatic change during the Palaeocene to Eocene based on fossil plants from Fushun, China. Palaeogeogr. Palaeoclimatol. Palaeoecol. 295, 323–331. https://doi.org/10.1016/j.palaeo.2010.06.010.
Wang, Q., Spicer, R.A., Yang, J., Wang, Y.F., Li, C.S., 2013. The Eocene climate of China, the early elevation of the Tibetan Plateau and the onset of the Asian Monsoon. Glob. Change Biol. 19, 3709–3728. https://doi.org/10.1111/gcb.12336.
Wang, Y., Luo, J., Xue, X., Korpelainen, H., Li, C., 2008. Diversity of microsatellite markers in the populations of *Picea asperata* originating from the mountains of China. Plant Sci. 168, 707–714. https://doi.org/10.1016/j.plantsci.2004.10.002.
West, C.K., Greenwood, D.R., Basinger, J.F., 2015. Was the Arctic Eocene 'rainforest' monsoonal? Estimates of seasonal precipitation from early Eocene megafloras from Ellesmere Island, Nunavut. Earth Planet. Sci. Lett. 427, 18–30. https://doi.org/10.1016/j.epsl.2015.06.036.
Westerhold, T., Marwan, N., Drury, A.J., Liebrand, D., Agnini, C., Anagnostou, E., Barnet, J.S.K., Bohaty, S.M., De Vleeschouwer, D., Florindo, F., Frederichs, T., Hodell, D.A., Holbourn, A., Kroon, D., Lauretano, V., Littler, K., Lourens, L.J., Lyle, M.W., Pälike, H., Röhl, U., Tian, J., Wilkens, R.H., Wilson, P.A., Zachos, J.C., 2020. An astronomically dated record of Earth's climate and its predictability over the last 66 million years. Science 369, 1383–1387. https://doi.org/10.1126/science.aba6853.
Wing, S.L., Harrington, G.J., Smith, F.A., Bloch, J.I., Boyer, D.M., Freeman, K.H., 2005. Transient floral change and rapid global warming at the Paleocene–Eocene boundary. Science 310, 993–996. https://doi.org/10.1126/science.1116913.
Wolfe, J.A., 1978. A paleobotanical interpretation of Tertiary climates in the Northern Hemisphere. Am. Sci. 66, 694–703.
Wu, G.X., Liu, Y., Wang, T., Wan, R., Liu, X., Li, W., Wang, Z., Liang, X., 2007. The influence of mechanical and thermal forcing by the Tibetan Plateau on Asian climate. J. Hydrometeorol. 8, 770–789.
Wu, G.X., Liu, Y., He, B., Bao, Q., Duan, A., Jin, F.F., 2012. Thermal controls on the Asian summer monsoon, 2012 Sci. Rep. 2 (1), 404. https://doi.org/10.1038/srep00404.
Xie, Y.L., Wu, F.L., Fang, X.M., 2019. Middle Eocene East Asian monsoon prevalence over southern China: evidence from palynological records. Glob. Planet. Change 175, 13–26. https://doi.org/10.1016/j.gloplacha.2019.01.019.
Yao, Y.F., Bera, S., Ferguson, D.K., Mosbrugger, V., Paudayal, K.N., Jin, J.H., Li, C.S., 2009. Reconstruction of paleovegetation and paleoclimate in the early and middle Eocene, Hainan Island, China. Clim. Change 92, 169–189. https://doi.org/10.1007/s10584-008-9457-2.
Zachos, J.C., Dickens, G.R., Zeebe, R.E., 2008. An early Cenozoic perspective on greenhouse warming and carbon-cycle dynamics. Nature 451, 279–283. https://doi.org/10.1038/nature06588.
Zhang, S., Wang, B., 2008. Global summer monsoon rainy seasons. Int. J. Clim. 28, 1563–1578. https://doi.org/10.1002/joc.1659.
Zhang, Z., Wang, H., Guo, Z., Jiang, D., 2007. What triggers the transition of palaeoenvironmental patterns in China, the Tibetan Plateau uplift or the Paratethys Sea retreat? Palaeogeogr. Palaeoclimatol. Palaeoecol. 245, 317–331. https://doi.org/10.1016/j.palaeo.2006.08.003.
Zhang, Z., Flatoy, F., Wang, H., Bethke, I., Bentsen, M., Guo, Z., 2012. Early Eocene Asian climate dominated by desert and steppe with limited monsoons. J. Asian Earth Sci. 44, 24–35. https://doi.org/10.1016/j.jseaes.2011.05.013.